6

Real-Time Full Color Multiband Night Vision

Alexander Toet and Maarten A. Hogervorst
TNO Human Factors
The Netherlands

1. Introduction

Night vision cameras are widely used for military and law enforcement applications related to surveillance, reconnaissance, intelligence gathering, and security. The two most common night-time imaging systems are low-light-level (e.g., image-intensified) cameras, which amplify the reflected visible to near infrared (VNIR) light, and thermal infrared (IR) cameras, which convert thermal energy from the midwave (3 to 5 microns) or the long wave (8 to 12 microns) part of the spectrum into a visible image. These systems create images with a single (one-dimensional) output per pixel. As a result their ability to discriminate different materials is limited. This can be improved by combining systems that are sensitive to different parts of the electromagnetic spectrum, resulting in multiband or hyperspectral imagers. The number of different outputs increases dramatically by combining multiple sensors (e.g. up to N^2 for two sensors, when the number of different outputs for each sensor is N), which in turn leads to a significant increase in the number of materials that can be discriminated. The combination of multiple bands allows for meaningful color representation of the system output. It is therefore not surprising that the increasing availability of fused and multiband infrared and visual nightvision systems (e.g. Bandara et al., 2003; Breiter et al., 2002; Cho et al., 2003; Cohen et al., 2005; Goldberg et al., 2003) has led to a growing interest in the (false) color display of night vision imagery (Li & Wang, 2007; Shi et al., 2005a; Shi et al., 2005b; Tsagaris & Anastasopoulos, 2006; Zheng et al., 2005).

In principle, color imagery has several benefits over monochrome imagery for surveillance, reconnaissance, and security applications. The human eye can only distinguish about 100 shades of gray at any instant. As a result, grayscale nightvision images are sometimes hard to interpret and may give rise to visual illusions and loss of situational awareness. Since people can discriminate several thousands of colors defined by varying hue, saturation, and brightness, a false color representation may facilitate nightvision image recognition and interpretation. For instance, color may improve feature contrast, thus enabling better scene segmentation and object detection (Walls, 2006). This may allow an observer to construct a more complete mental representation of the perceived scene, resulting in better situational awareness. It has indeed been found that scene understanding and recognition, reaction time, and object identification are faster and more accurate with color imagery than with monochrome imagery (Cavanillas, 1999; Gegenfurtner & Rieger, 2000; Goffaux et al., 2005; Oliva & Schyns, 2000; Rousselet et al., 2005; Sampson, 1996; Spence et al., 2006; Wichmann et al., 2002). Also, observers are able to selectively attend to task-relevant color targets and to

ignore non-targets with a task-irrelevant color (Ansorge et al., 2005; Folk & Remington, 1998; Green & Anderson, 1956). As a result, simply producing a false color nightvision image by mapping multiple spectral bands into a three dimensional color space already generates an immediate benefit, and provides a method to increase the dynamic range of a sensor system (Driggers et al., 2001). However, the color mapping should be chosen with care and should be adapted to the task at hand. Although general design rules can be used to assure that the information available in the sensor image is optimally conveyed to the observer (Jacobson & Gupta, 2005), it is not trivial to derive a mapping from the various sensor bands to the three independent color channels, especially when the number of bands exceeds three (e.g. with hyperspectral imagers; Jacobson et al., 2007). In practice, many tasks may benefit from a representation that renders a nighttime scene in daytime colors. Jacobson & Gupta (Jacobson et al., 2007; Jacobson & Gupta, 2005) therefore advise to use a consistent color mapping according to a natural palette. The use of natural colors facilitates object recognition by allowing access to stored color knowledge (Joseph & Proffitt, 1996). Experimental evidence indicates that object recognition depends on stored knowledge of the object's chromatic characteristics (Joseph & Proffitt, 1996). In natural scene recognition paradigms, optimal reaction times and accuracy are obtained for normal natural (or diagnostically) colored images, followed by their grayscale version, and lastly by their (nondiagnostically) false colored version (Goffaux et al., 2005; Oliva, 2005; Oliva & Schyns, 2000; Rousselet et al., 2005; Wichmann et al., 2002). When sensors operate outside the visible waveband, artificial color mappings generally produce false color images whose chromatic characteristics do not correspond in any intuitive or obvious way to those of a scene viewed under natural photopic illumination (e.g. (Fredembach & Süsstrunk, 2008)). As a result, this type of false color imagery may disrupt the recognition process by denying access to stored knowledge. In that case observers need to rely on color contrast to segment a scene and recognize the objects therein. This may lead to a performance that is even worse compared to single band imagery alone (Sinai et al., 1999a). Experiments have indeed convincingly demonstrated that a false color rendering of night-time imagery which resembles natural color imagery significantly improves observer performance and reaction times in tasks that involve scene segmentation and classification (Essock et al., 1999; Sinai et al., 1999b; Toet & IJspeert, 2001; Vargo, 1999; White, 1998), whereas color mappings that produce counterintuitive (unnaturally looking) results are detrimental to human performance (Krebs et al., 1998; Toet & IJspeert, 2001; Vargo, 1999). One of the reasons often cited for inconsistent color mapping is a lack of physical color constancy (Vargo, 1999). Thus, the challenge is to give nightvision imagery an intuitively meaningful ("naturalistic") and stable color appearance, to improve the viewer's scene comprehension and enhance object recognition and discrimination (Scribner et al., 1999). Several techniques have been proposed to render night-time imagery in color (e.g. (Sun et al., 2005; Toet, 2003; Tsagiris & Anastassopoulos, 2005; Wang et al., 2002; Zheng et al., 2005)). Simply mapping the signals from different nighttime sensors (sensitive in different spectral wavebands) to the individual channels of a standard color display or to the individual components of perceptually decorrelated color spaces, sometimes preceded by principal component transforms or followed by a linear transformation of the color pixels to enhance color contrast, usually results in imagery with an unnatural color appearance (e.g. Howard et al., 2000; Krebs et al., 1998; Li et al., 2004; Schuler et al., 2000; Scribner et al., 2003). More intuitive color schemes may be obtained through opponent processing through feedforward center-surround shunting neural

networks similar to those found in vertebrate color vision (Aguilar et al., 1998; Aguilar et al., 1999; Fay et al., 2000a; Fay et al., 2000b; Huang et al., 2007; Warren et al., 1999; Waxman et al., 1995a; Waxman et al., 1997). Although this approach produces fused nighttime images with appreciable color contrast, the resulting color schemes remain rather arbitrary and are usually not strictly related to the actual daytime color scheme of the scene that is registered. In the next section we give an overview of some recently developed color mapping schemes that can give false color multiband nightvision imagery a natural color appearance. First we present a simple false color mapping scheme that is inspired by previous color opponent processing schemes. Although this scheme produces fused false color images with large color contrast and preserves the identity of the input signals (thus making the images perceptually intuitive), the resulting color representation is not strictly natural looking (Toet & Walraven, 1996). We therefore developed a statistical extension of this coloring method which produces colorized multiband nightvision imagery with a regular daylight color appearance (Toet, 2003). This mapping transfers the first order statistics of the color distribution of a given color reference image to the multiband nighttime images, thereby giving them a similar color appearance as the reference image. In its original form this method is computationally expensive. However, computational simplicity (enabling real-time implementation) can be achieved by applying the statistical mapping approach in a lookup-table framework. Although the statistical mapping approach yields a natural color rendering, it achieves no color constancy, since the mapping depends on the relative amounts of the different materials in the scene (and will therefore change when the camera pans over or zooms in on a scene). We therefore developed a sample-based color mapping scheme that yields both color constancy and computational efficiency (Hogervorst & Toet, 2008a; Hogervorst & Toet, 2008b; Hogervorst & Toet, 2010). In contrast to the statistical color mapping method, the sample based color transfer method (for which a patent application is currently pending: Hogevorst et al., 2006) is highly specific for different types of materials in the scene and can easily be adapted for the task at hand, such as the detection of camouflaged objects. After explaining how the sample based color transformation can be derived from the combination of a given multi-band sensor image and a corresponding daytime reference image, we will dicuss how it can be deployed at night and implemented in real-time.

2. Color mapping

2.1 Center-surround opponent-color fusion

Opponent color image fusion was originally developed at the MIT Lincoln Laboratory (Gove et al., 1996; Waxman et al., 1995a; Waxman et al., 1996a; Waxman et al., 1996b; Waxman et al., 1997; Waxman et al., 1999) and derives from biological models of color vision (Schiller, 1982; Schiller, 1984; Schiller et al., 1986; Schiller, 1992) and fusion of visible light and infrared (IR) radiation (Newman & Hartline, 1981; Newman & Hartline, 1982).

In the case of color vision in monkeys and man, retinal cone sensitivities are broad and overlapping, but the images are contrast enhanced *within* bands by spatial opponent processing (via cone-horizontal-bipolar cell interactions) creating both ON and OFF center-surround response channels (Schiller, 1992). These signals are then contrast enhanced *between* bands via interactions among bipolar, sustained amacrine, and single-opponent-color ganglion cells (Gouras, 1991; Schiller & Logothetis, 1990), all within the retina. Further

color processing in the form of double-\-opponent-color cells is found in the primary visual cortex of primates (and the retinas of some fish). Opponent processing interactions form the basis of such percepts as color opponency, color constancy, and color contrast, though the exact mechanisms are not fully understood. Double-opponent-color processing has been applied to multispectral IR target enhancement (Gove et al., 1996; Waxman et al., 1995b).
Fusion of visible and thermal imagery has been observed in several classes of neurons in the optic tectum (evolutionary progenitor of the superior colliculus) of rattlesnakes (pit vipers), and pythons (boid snakes), as described by (Newman & Hartline, 1981; Newman & Hartline, 1982). These neurons display interactions in which one modality (e.g. IR) can enhance or depress the response to the other sensing modality (e.g. visible) in a strongly nonlinear fashion. Such interactions resemble opponent-processing between bands as observed in primate retina.
For opaque surfaces in thermodynamic equilibrium, spectral reflectivity ρ and emissivity ε are linearly related at each wavelength λ: $\rho(\lambda) = 1 - \varepsilon(\lambda)$. This provides a rationale for the use of both on-center and off-center channels when treating infrared imagery as characterized by thermal emissivity (Toet et al., 1997).
In the opponent-color image fusion methodology the individual input images are first enhanced by filtering them with a feedforward center-surround shunting neural network (Grossberg, 1988). This operation serves

1. to enhance spatial contrast in the individual visible and IR bands,
2. to create both positive and negative polarity IR contrast images, and
3. to create two types of single-opponent-color contrast images.

The resulting single-opponent-color contrast images represent grayscale fused images that are analogous to the IR-depressed visual and IR-enhanced visual cells of the rattlesnake (Newman & Hartline, 1981; Newman & Hartline, 1982).

2.2 Pixel based opponent-color fusion

Inspired by the opponent-color fusion approach (Waxman et al., 1995a; Waxman et al., 1996a; Waxman et al., 1996b; Waxman et al., 1997; Waxman et al., 1999), we derived a simplified (pixel based) version of this method, which fuses visible and thermal images into false color images with a relatively natural or intuitive appearance.
Let I_1 and I_2 be two input images with the same spatial resolution and dynamic range. The common component of both signals is computed as the morphological intersection:

$$I_1 \cap I_2 = \mathrm{Min}\{I_1, I_2\} \tag{1}$$

The unique or characteristic component I^* of each image modality remains after subtraction of the common component:

$$I_1^* = I_1 - I_1 \cap I_2 \quad ; \quad I_2^* = I_2 - I_1 \cap I_2 \tag{2}$$

The characteristic components are emphasized in the fused image by subtracting them from the opposite image modalities. The color fused image is then obtained by mapping these differences to respectively the red and green bands of a RGB false color image. The characteristic components of both image modalities can be further emphasized by mapping their difference to the blue band of the fused false color image, so that the final mapping is given by (Toet & Walraven, 1996):

$$\begin{pmatrix} \mathrm{R} \\ \mathrm{G} \\ \mathrm{B} \end{pmatrix} = \begin{pmatrix} I_2 - I_1^* \\ I_1 - I_2^* \\ I_2^* - I_1^* \end{pmatrix} \tag{3}$$

In case of visual and thermal input images, I_1 = Vis and I_2 = *IR*. Because the method is computationally simple it can implemented in hardware or even be applied in real-time using standard processing equipment (Aguilar et al., 1998; Aguilar et al., 1999; Waxman et al., 1999). The resulting color rendering enhances the visibility of certain details and preserves the specificity of the sensor information. In addition, it has a fairly natural color appearance (Fig. 1 and Fig. 2). The resulting images agree with our natural associations of warm (red) and cool (blue). To further enhance the appearance of the fused results, the R, G, B channels can be input to a color remapping stage in which, following conversion to H, S, V (hue, saturation, value) color space, hues can be remapped to alternative "more natural'" hues, colors can be desaturated, and then reconverted back to R, G, B signals to drive a color display. Because of the enhanced color contrast and its intuitive appearance this color fused image representation is expected to improve both visual target detection and recognition performance are expected to benefit in terms of both speed and precision. Two observer studies were performed to test this hypothesis.

In the first observer study we used grayscale intensified visual and thermal images, and color fused motion sequences, depicting scenes in which a person walked across a rural scene with man-made objects (Toet et al., 1997). The reference (terrain) features were represented with high contrast in the intensified visual images (Fig. 2a) and low contrast in

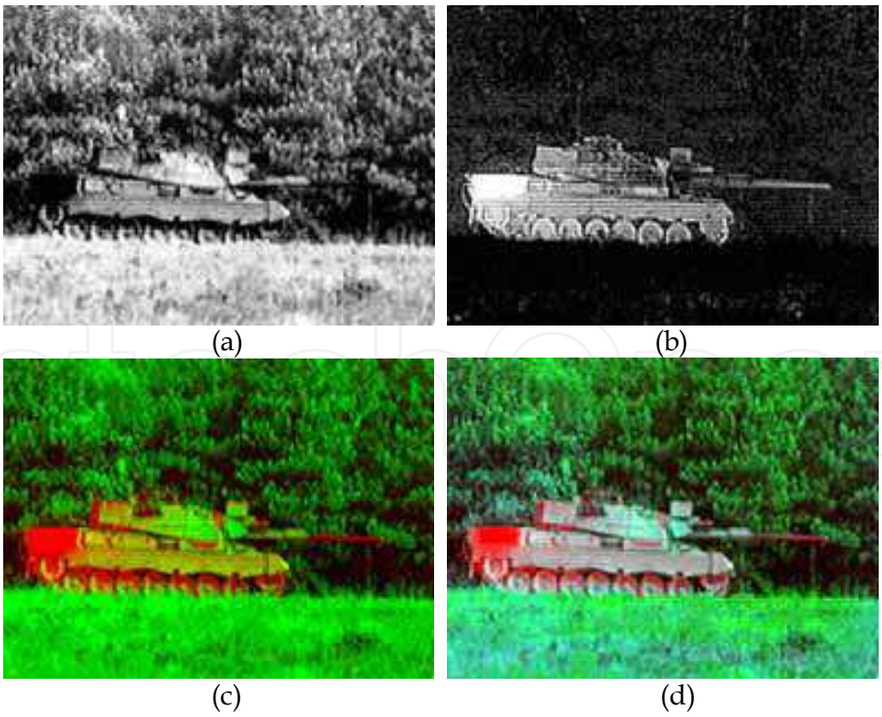

(a) (b) (c) (d)

Fig. 1. Visual (a) and thermal (b) input images. (c) Result of mapping (a) and (b) to respectively the green and red channels of an RGB display. (d) Result of the mapping defined by equation.

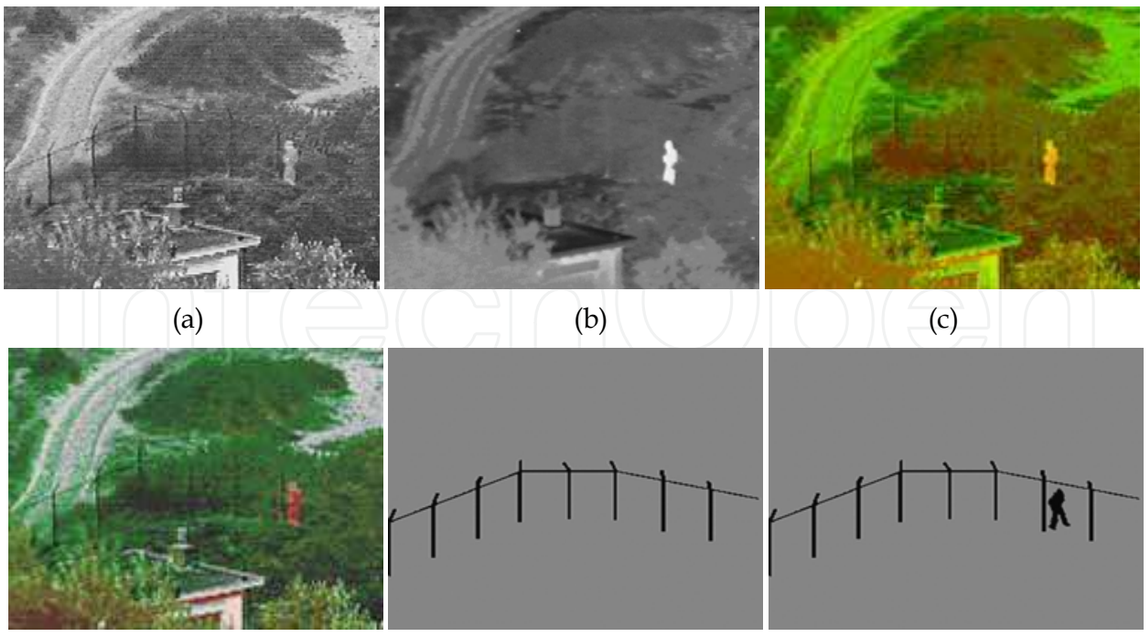

(a) (b) (c)

(d) (e) (f)

Fig. 2. Scene representing a person walking along the outside of a fence. Visual (a) and thermal (b) input images. (c) Result of mapping (a) and (b) to respectively the green and red channels of an RGB display. (d) Result of the mapping defined in equation . (e) Reference image used in the spatial localization task. (f) Image used to assess baseline localization performance.

the thermal images (Fig. 2b), while the opposite was the case for the image of the person. All details were represented in the color fused images (Fig. 2d). During the localization experiments, individual frames from the motion sequences and for each of the three image modalities (visual, thermal and color fused) were briefly (1 s) and in random order presented to human observers. After the presentation of each frame a schematic grayscale image was shown representing only the reference features on a homogeneous background (e.g. Fig. 2e). Observers were asked to indicate the perceived position of the person in the scene by placing a mouse controlled cursor at the corresponding location in the schematic reference image. The position of the reference image on the display screen was given a small random variation to prevent participants from using cues from afterimages. Baseline performance was assessed using schematic images, similar to the reference image, but with a binary image of the person at his actual location in the corresponding frames (e.g. Fig. 2f). The results show that observers can localize a person in a scene with a significantly higher accuracy and with greater confidence when they perform with color fused images, compared to the individual image modalities (visible and thermal; Toet et al., 1997).

In the second observer study we used grayscale visual and thermal (8-12 μm) motion sequences, and color fused motion sequences, depicting a mountain range in the background and grasslands in the foreground, with infantry soldiers, vehicles, and a smoke screen (Fig. 3). The visual and thermal motion sequences are a subset (images 37--93) of the MS01 Test Sequence that consists of 110 corresponding image pairs, registered at CFB Valcartier (Sévigny, 1996). Both a tow truck and a helicopter move across the scene during the registration period. The infantry soldiers are not visible in the visual images (Fig. 3a-c),

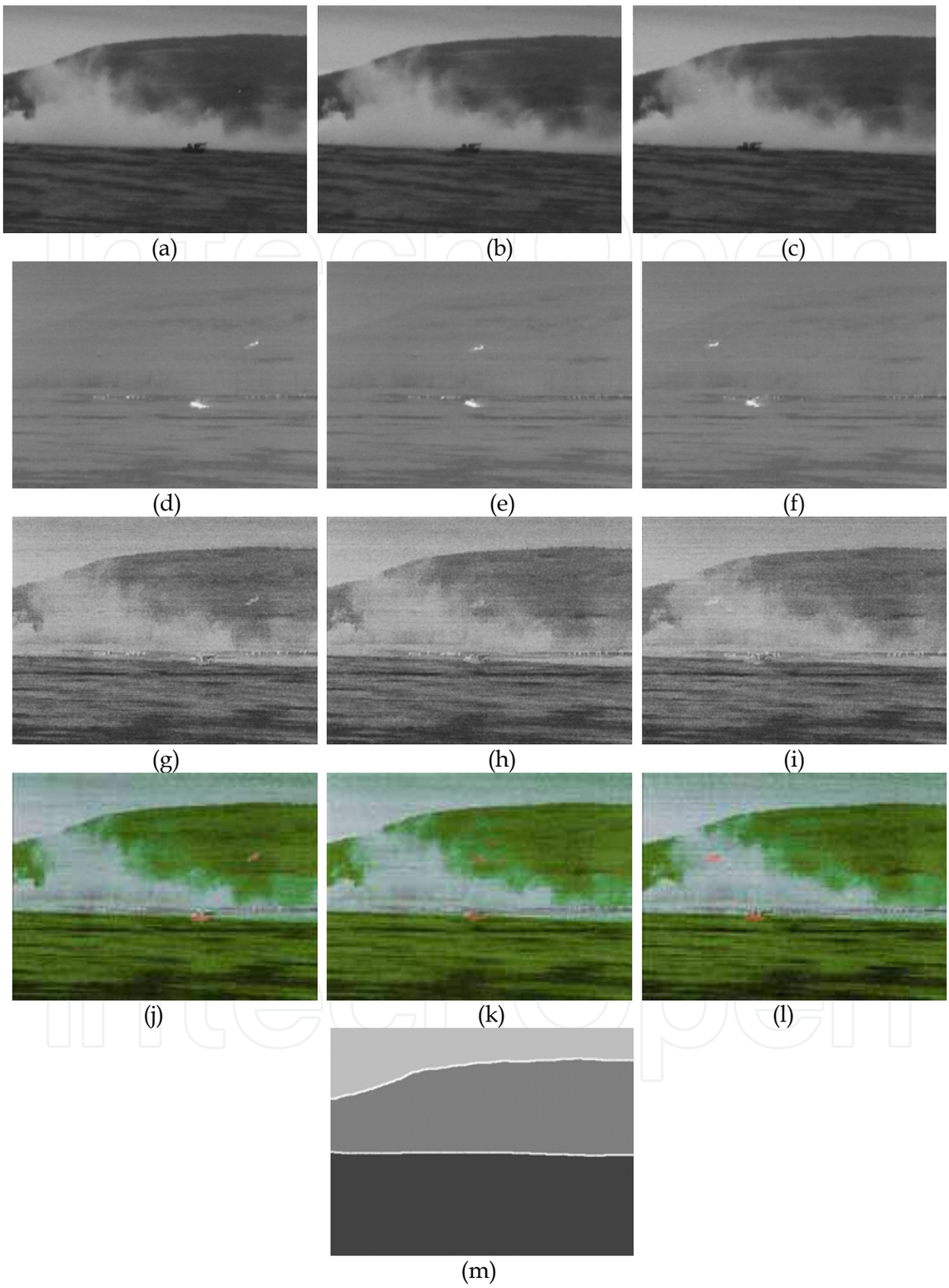

Fig. 3. Left to right: successive frames of a time sequence. Top-down: video (a-c), thermal (d-f), grayscale fused (g-i), and color fused (j-l) images. (m) Schematic reference image.

because they are obscured by the smoke screen. However, they can easily be perceived in the thermal images (Fig. 3d-f), where they appear as small hot spots. In the visual images, the visibility of the helicopter ranges from barely visible to not visible (when it flies behind the smoke screen: Fig. 3f). In the thermal images there is almost no contrast between the foreground (grassland) and the background (the mountain range). Also, the mountain range and the sky have little contrast in the thermal images (the skyline of the mountain range is barely visible). The contrast between the sky and the top of the mountain range is much larger in the CCD images. The visual and thermal images were color fused using equation 3 (see Fig. 3j-l). Fig. 3g-i shows the luminance component of Fig. 3j-l. Both the graylevel fused (Fig. 3g-i) and the color fused (Fig. 3j-l) images represent all details of interest. However, in the grayfused images, where details are represented by different shades of gray, it is sometimes hard to visually segment the scene, because there are no visible boundaries (edges) between different physical objects with the same mean luminance. For instance, in the visual images the smokescreen has a high luminance (is very bright). In the thermal images, the warmer (barren) parts of the grassland and the helicopter are represented as bright regions. As a result, there is sometimes very little contrast in the grayfused images between the smokescreen and respectively the helicopter and the grassland. In the color fused images, the additional color contrast leads to an effortless perceptual segmentation of the scene. We measured the accuracy with which observers can determine the position of the helicopter in a briefly (600 ms) presented motion sequence, for visual, thermal, and color fused image sequences. Only a limited portion (a restricted field of view) of the entire scene was displayed during each test interval. The field of view was randomly positioned on the dynamic battlefield scene. This experimental paradigm simulates a field of view search of the display of a moving camera scanning over a larger field of regard. For each individual frame a corresponding reference image was constructed, representing a segmented version of the background of the original scene (mountain range, grassland, and sky; see Fig. 3m). After watching each movie fragment, observers were asked to indicate the location where the helicopter was last seen, by placing a mouse-controlled cursor over the schematic reference image. This task requires observers to quickly determine *(a)* the location of reference contours, and *(b)* the location of the target at each stimulus presentation. This involves rapid visual scene segmentation. The performance in this relative spatial localization task depends on the accuracy with which the position of the helicopter can be perceived relative to the contours of the mountain range. The results of this experiment show that the accuracy with which observers can determine the position of a helicopter in a briefly presented and randomly positioned window on a dynamic battlefield scene is significantly higher for color fused images than for the individual visual and thermal images (Toet et al., 1997). The color fused images probably represent all relevant features at a sufficiently large perceptual contrast to allow rapid visual identification of the spatial layout of the scene, thereby enabling subjects to perform the task. We also observed that a restriction of the field of view results in a significant increase in the localization error for the visual and thermal image modalities, but not for the fused image modalities.

The false color mapping defined by equation 3 has also been successfully applied in other domains, like the fusion of retinal images (Kolar et al., 2008; Laliberté et al., 2002; Laliberté et al., 2003) and the fusion of infrared and synthetic images (Simard et al., 1999; Simard et al., 2000).

In ophthalmology, visual fundus images are often used in combination with fluorescein angiogram images. Visual images of the retina clearly represent hard exudates. Fluorescein

angiogram images represent the macula, the arteries and veins at high contrast, thus allowing the detection of occluded and leaking capillaries, microaneurims, macular edema, and neovascularization. Using the mapping defined by equation 3 to fuse visual fundus images with fluorescein angiogram images provides better color contrast rendering than other opponent-color fusion methods, thus enhancing diagnostic performance and reducing visual workload (Laliberté et al., 2002; Laliberté et al., 2003). It was for instance found that this mapping clearly represents neovessels and depicts the macula at high contrast (Laliberté & Gagnon, 2006) Fig. 4. shows two examples of the fusion of grayscale visual fundus images (Fig. 4a and d) with corresponding fluorescein angiogram images (Fig. 4b and e). The fused images (Fig. 4c and f) represent the interesting details like the vascular network (purple veins) and the exudates (yellow lesions) with large color contrast. When using equation 3 to fuse thermal and autofluorescent images of the retina (Kolar et al., 2008), the resulting false color images provide higher contrast for the hyperfluent areas of the autofluorescent images (which are symptoms for glaucoma in its early stages) and clearly represent the position of the optic nerve head from the infrared image.
Simulated flight tests with fused infrared and synthetic imagery showed that the fusion technique defined by equation 3 preserves all features relevant for obstacle avoidance, and significantly improves detection distances for all simulated visibility conditions (Simard et al., 1999; Simard et al., 2000).

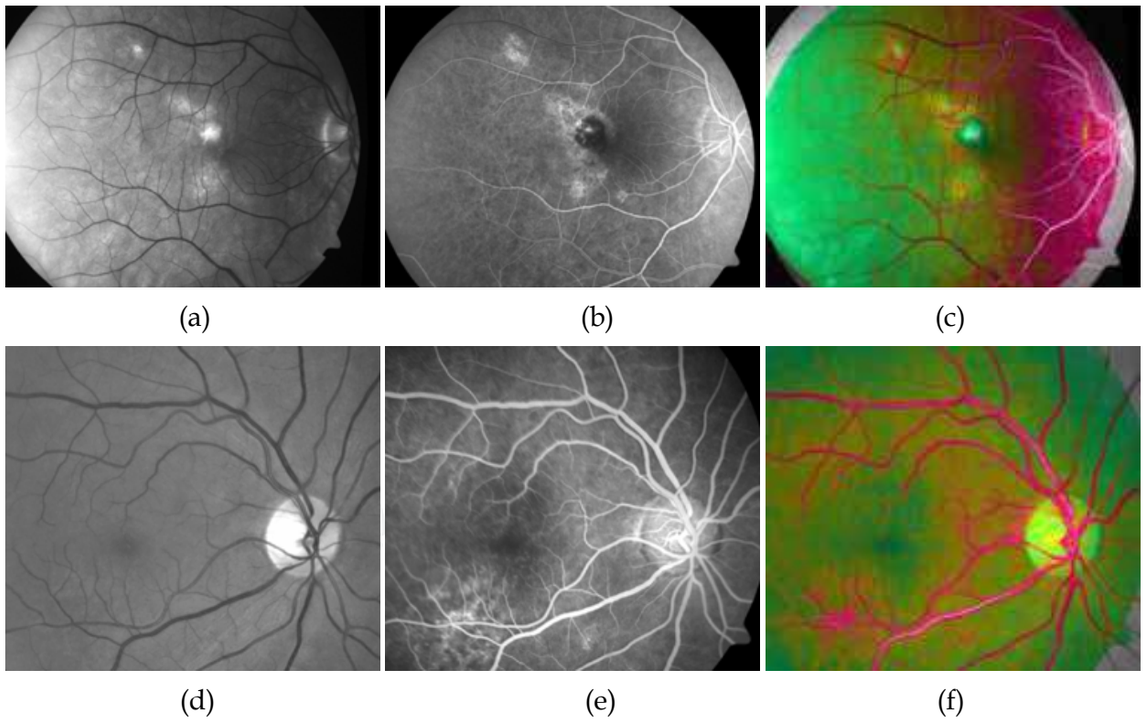

Fig. 4. Photographs (a,d) and fluorescein angiogram images (b,e) and their color fused representation (c,f).

2.3 Statistical color transform

Although the overall color appearance of images produced with the opponent-color fusion scheme is fairly intuitive, some details may still be depicted with unnatural colors. In this

section we present a method that gives multiband nighttime images the appearance of regular daylight color images by transferring the first order color statistics from full color daylight imagery to the false color multiband nightvision imagery. The method is based on a technique that was developed to enhance the color representation of synthetic imagery (Reinhard et al., 2001). The outline of the method is as follows. As input the method requires a false color RGB image. This can be produced by mapping the 2 or 3 individual bands (or the first 2 or 3 principal components when the sensor system delivers more than 3 bands) of a multiband nightvision system to the respective channels of an RGB image. Next, the false color RGB nightvision image and a regular full color daylight reference image are both transformed into the perceptually decorrelated *laβ* opponent color space (Ruderman et al., 1998). Then, the mean and standard deviation of each of the 3 color channels of the multiband nightvision image are set equal to those of the reference image:

$$\begin{aligned} l^* &= \frac{\sigma_r^l}{\sigma^l}\left(l - \langle l \rangle\right) \\ \alpha^* &= \frac{\sigma_r^\alpha}{\sigma^\alpha}\left(\alpha - \langle \alpha \rangle\right) \\ \beta^* &= \frac{\sigma_r^\beta}{\sigma^\beta}\left(\beta - \langle \beta \rangle\right) \end{aligned} \tag{4}$$

where $\langle\ \rangle$ denotes the mean, σ the standard deviation, and the index *r* refers to the reference image.

Finally, the multiband nightvision image is transformed back to RGB space for display. The result is a full color representation of the multiband nightvision image with a color appearance that closely resembles the color appearance of the daylight reference image. The daylight reference image should display a scene which is similar (but not necessarily identical to) the one displayed by the multiband nightvision image. The order of the mapping is irrelevant, since the following procedure effectively rotates the color coordinate axes of the false color multiband nightvision images such that these will be aligned with the axes of the referenced daylight color image in the final result.

The statistical color transform is computationally expensive and therefore not suitable for real-time implementation. Moreover, although it can give multiband nighttime imagery a natural daylight color appearance, it can not achieve color constancy for dynamic imagery (Zheng & Essock, 2008), because the actual mapping depends on the relative amounts of different materials in (i.e. the composition or statistics of) the scene. Large objects in the scene will dominate the color mapping. As a result, the color of objects and materials may change over time when the sensor system pans over (or zooms in on) a given scene. We therefore developed a fixed lookup table based version of this statistical color mapping which is *(1)* computationally efficient, so that it can easily be deployed in real time, and which *(2)* yields constant object colors.

The new lookup table based statistical color transfer approach is illustrated in Fig. 5. for a multi-band image consisting of two channels. First, the two sensor images are mapped on two of the three channels of an RGB image. In this particular example (Fig. 5c) the visual band is (arbitrarily) mapped to R (red channel) and the near-infrared band is mapped to G (green channel). The result is the red-green false-color representation of the multi-band

(a) (b) (c)

(d) (e)

Fig. 5. Visible (a) and near infrared (b) image. (c) False color image obtained by assigning (a) to the green and (b) to the red channel of an RGB false color image (the blue channel is set to zero). The inset in this figure represents all possible combinations of signal values that can occur in the two sensor bands (upper left: both sensors give zero output; lower right: both sensors give maximal output). (d) Arbitrary reference daylight color image. (e) Result of mapping the first order statistics of the reference image (d) to the false color nighttime image (c). The inset in this figure represents the result of applying the same transform to the inset of (c), and shows all possible colors that can occur in the recolored sensor image (i.e. after applying the color mapping).

image shown in Fig. 5c. The statistical color transform can then be derived from the first order statistics of respectively *(a)* Fig. 5c and *(b)* a given daylight color reference image, like the one shown in square inset in Fig. 5d. The application of this statistical color transform to an input table of 2-tuples representing all possible sensor output values yields an output table containing all possible color values that can occur in the colorized nighttime image. The in- and output table pair defines the statistical color mapping and can therefore be deployed in a color lookup table transform procedure. The square inset in Fig. 5c represents the table of all possible two-band signal values as different shades of red, green and yellow. Application of the statistical color transform to the inset in Fig. 5c yields the inset shown in Fig. 5e. In a lookup table paradigm the insets in Fig. 5c and Fig. 5e together define the statistical color mapping. For any color in the false-color representation of Fig. 5c the corresponding color after application of the statistical color transform can easily be found by

(1) locating the color in the inset of Fig. 5c, and *(2)* finding the color at the corresponding location in the transformed inset in Fig. 5e. For instance, a pixel representing a high response in the visual channel and low response in the near infrared channel is represented with a red color (high value of red, low value of green) in the inset in Fig. 5c. In the inset of Fig. 5e the same pixel appears in a brownish color. The color transformation can thus be implemented by using the inset pair of Fig. 5c and Fig. 5e as color lookup tables. Then, the false color image Fig. 5c can be transformed into an indexed image using the red-green color lookup table (the inset of Fig. 5c). Replacing the color lookup table of the indexed image Fig. 5c by the transformed color lookup table (the inset of Fig. 5e) then transforms Fig. 5c into Fig. 5e. Note that the color mapping scheme is fully defined by the two color lookup tables. When all possible combinations of an 8-bit multi-band system are represented, these color lookup tables contain 256x256 entries. When a color lookup table with less entries is used (e.g. only 256), the color mapping can be achieved by determining the closest match of the table entries to the observed multi-band sensor values.

Once the color mapping has been derived from a multi-band nighttime image and its corresponding reference image, and once it has been defined as a lookup table transform, it can be applied to different and dynamic multi-band images. The advantage of this method is that the color of objects only depends on the multi-band sensor values and is independent of the image content. Therefore, objects keep the same color over time when registered with a moving camera. Another advantage of this implementation is that it requires minimal computing power. Once the color transformation has been derived and the pair of color lookup tables that defines the mapping has been created, the new color lookup table transform can be used in a (real-time) application.

2.4 Sample based color transform

In spite of all the afore-mentioned advantages of the lookup table based statistical color transform, there is still room for improvement. For instance, in this paradigm there is no strict relationship between sensor output values and object color, since the statistical approach inherently only addresses the global color characteristics of the depicted scene. In this section we will describe an alternative lookup table based method for applying natural colors to multi-band images, which alleviates this problem since it does not rely on image statistics. The color transformation is derived from a corresponding set of samples for which both the multi-band sensor values and the corresponding natural color (RGB-value) are known (Hogervorst et al., 2006). We will show that this method results in rendered multi-band images with colors that match the daytime colors more closely than the result of the statistical approach. In contrast to the statistical method, the derivation of the color mapping requires a registered image pair, consisting of a multi-band image and a daytime reference image of the same scene, sine the pixels serve as samples in this approach. Once the color mapping has been derived it can be applied to different multi-band nighttime images. Again, we will implement the color transformation using a color lookup table transformation, thus enabling real-time implementation.

The method is as follows. Given a set of samples (pixels) for which both the multi-band sensor output and the corresponding daytime colors are known, the problem of deriving the optimal color transformation is to find a transformation that optimally maps the N-dimensional (e.g. in our examples N = 2) multi-band sensor output vectors (one for each sample) to the 3-D vectors corresponding to the daytime colors (RGB). The mapping should

minimize the difference between the modeled colors and the measured colors. Moreover, the transformation should predict the mapping of untrained samples. Several methods exist to derive a suitable mapping, such as neural networks and support vector machines. What constitutes a suitable mapping is determined by the function that is minimized. Also the statement that the difference between the modeled colors and the measured colors is minimized should be formalized. We will minimize the average perceptual color difference between the modeled color and the measured color. More precisely, we will minimize the average squared distance between the perceptual color vectors *laβ* (see (Ruderman et al., 1998)). We will describe a (relatively) simple implementation that is not focused towards finding the theoretical optimum mapping, but that will lead to robust and good results and can be understood intuitively. We will now describe our new method for deriving a natural color transformation using the example shown in Fig. 6. Fig. 6a depicts the full color daytime reference image, which is in this case a color photograph taken with a standard digital camera. Figs. 6b and c respectively show a visible and near-infrared image of the same scene. Fig. 6f shows the result of applying daytime colors to the two-band night-time sensor image using our new color mapping technique.

The method works as follows. First, the multi-band sensor image is transformed to a false-color image by taking the individual bands (Fig. 6b and c) as input to the R and G channels (and B when the sensor contains three bands), referred to as the RG-image (Fig. 6e). In practice any other combination of 2 channels can also be used (one could just as well use the combinations R & B or B & R). Mapping the two bands to a false color RGB-image allows us to use standard image conversion techniques, such as indexing. In the next step the resulting false color (RG-image) Fig. 6e is converted to an indexed image. Each pixel in such an image contains a single index. The index refers to an RGB-value in a color lookup table (the number of entries can be chosen by the user). In the present example of a sensor image consisting of two bands (R and G; Fig. 6e) the color lookup table contains various combinations of R and G values (the B-values are zero when the sensor or sensor pair provides only two bands). For each index representing a given R,G combination (a given false color) the corresponding natural color equivalent is obtained by locating the pixels in the target image with this index and finding the corresponding pixels in the (natural color) reference image (Fig. 6a). First, the RGB-values are converted to perceptually de-correlated *laβ* values (see (Ruderman et al., 1998)). Next, we calculate the average *laβ*-vector over this ensemble of pixels. This assures that the computed average color reflects the perceptual average color. Averaging automatically takes the distribution of the pixels into account: colors that appear more frequently are attributed a greater weight. Let us for instance assume that we would like to derive the natural color associated with index 1. In that case we locate all pixels in the (indexed) false color multi-band target image with index 1. We then take all corresponding pixels in the reference daytime color image, convert them to *laβ*, and calculate the average *laβ*-value. Next, we transform the resulting average *laβ*-value back to RGB. Finally, we assign this RGB-value to index 1 of the new color lookup table. These steps are successively carried out for all indices. This process yields a new color lookup table containing the natural colors associated with the various multi-band combinations in the false color (RG) color lookup table. Replacing the RG-color lookup table (left side of Fig. 6d) by the color lookup table with natural colors (right side of Fig. 6d) yields an image with a natural color appearance, in which the colors are optimized for this particular sample set (Fig. 6d). Note that the red parts in the scene in Fig. 6a do not turn out red again in the

rendered night-time image Fig. 6f. This is due to the fact that other materials which occupy a larger area of the scene (and which therefore dominate the color mapping) give the same sensor output in the two bands. Also, the red flags are not apparent in the visible band (Fig. 6b). This has only a minor effect on the overall appearance of the scene as long as the parts that change between the different band recordings occupy only a relatively small area.

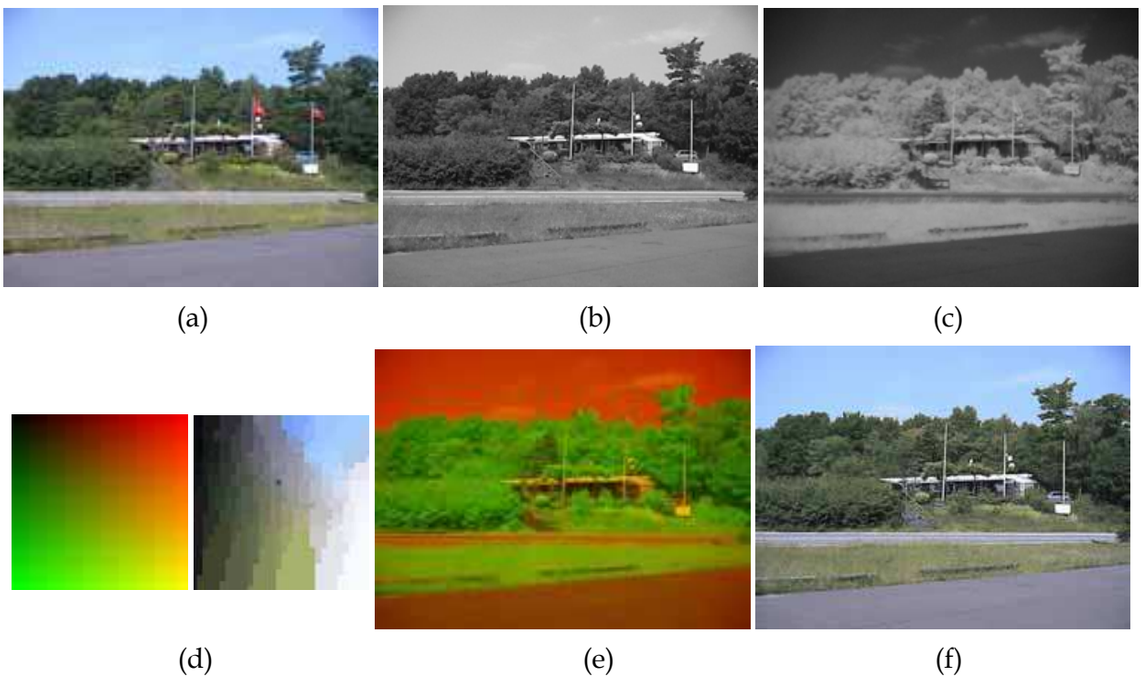

(a) (b) (c)

(d) (e) (f)

Fig. 6. (a) Natural daylight color reference image. Visible (b) and near-infrared (c) images of the same scene. (d) The color mapping derived from corresponding pixel pairs in a and b-c. (e) Combined RG false color representation of (b) and (c), obtained by assigning (b) to the green and (c) to the red channel of an RGB color image (the blue channel is set to zero). (f) Result of the application of the mapping scheme in (d) to the two band false color image in (e).

Fig. 7 illustrates the difference between the statistical and the sample based color transforms. In this example we determined a color mapping lookup table from a pair of images consisting of (Fig. 7a) the original version of a full color daylight photograph and (Fig. 7b) the same image from which the blue channel has been removed (B=0). Note that the sample-based color remapping (Fig. 7c), using the sample based color lookup table (inset) determined from the image pair Fig. 7a and Fig. 7b, nicely restores most of the blue hues in the scene, while the statistical color remapping procedure (Fig. 7d) is not capable to restore the missing information. This is due to the fact that the sample-based method allows for nonlinear transformations while the statistical method is a linear (affine) transformation (in CIELAB-color space).

Fig. 8a and b show respectively visual and near-infrared images of the same scene. Fig. 8c shows the red-green false color representation of Fig. 8a and b. Fig. 8d shows the daytime reference image corresponding to the multi-band sensor image. Straightforward application of the sample-base color transform results in Fig. 8e. Note that the colors of this figure closely match the daytime colors as shown in Fig. 8d (e.g. the sky is blue). However, the

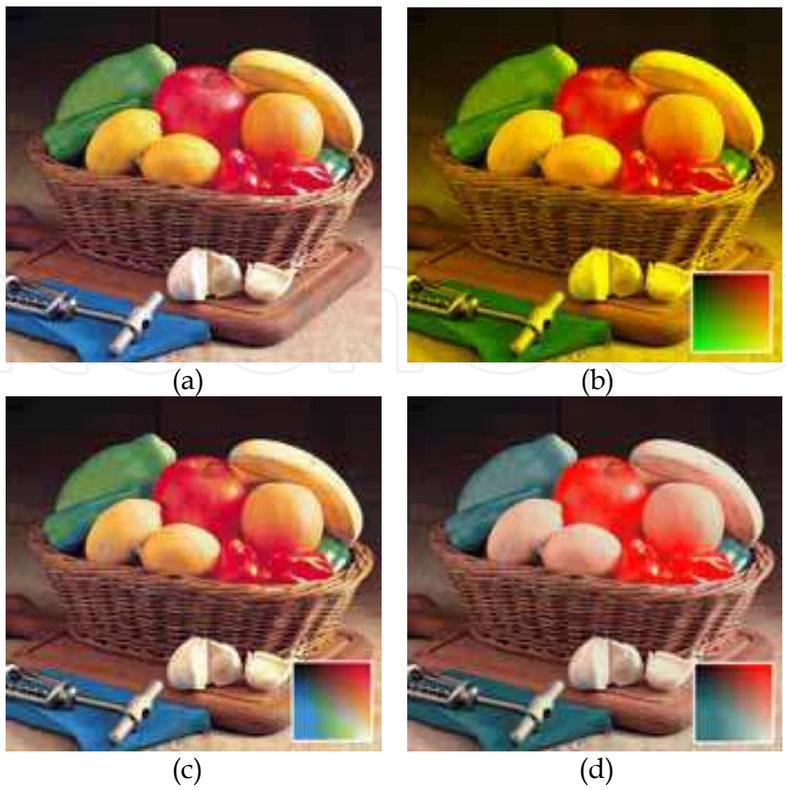

Fig. 7. (a) Full color RGB image. (b) Image from (a) after removal of the blue band (B=0). (c) Result of sample-based color remapping, using the color lookup table (inset) determined from the image pair (a,b). (d) Result of the statistical color remapping procedure.

image looks noisy and certain objects appear in the wrong color (e.g. the bench and parts of the roof). This is due to the fact that the luminance in the colorized image does not increase continuously with increasing sensor output (the luminance value in Fig. 8c). This gives an undesirable "solarizing" effect. We therefore derived from this color map (inset in Fig. 8e) another color map (inset in Fig. 8f) in which the luminance increases linearly with the distance to the top-left corner. Fig. 8f shows the result of this new color mapping. The colors in Fig. 8f closely match the daytime colors. The sky is dark instead of light-blue. This corresponds to the intuition that the sky should look dark at night, and does not affect the situational awareness. Also important is the fact that the color transformation shown in Fig. 8f is smooth, in contrast to the one shown in Fig. 8e. Intuitively a small variation in sensor output should lead to a small color change, i.e. a smooth color transformation is expected to lead to better matching colors when applied to other multi-band sensor images. Also, with smooth color transformations noise leads to less clutter. Furthermore, the color fused result provides a better impression of the depth in the scene (compare e.g. Fig. 8b and 8f).

Fig. 9a-c shows the result of applying the same lookup-table transform to multi-band sensor images of different scenes, together with the corresponding daytime full color images (Fig. 9d-f). Although the colors do not always fully match the daytime colors, they are still characteristic for the different materials displayed in the scene. Thus, the colorized fused image facilitates interpretation of the scene (situational awareness).

Dedicated color mapping schemes can be derived that are optimally tuned for different environments. When deploying the color transfer method at night an appropriate color

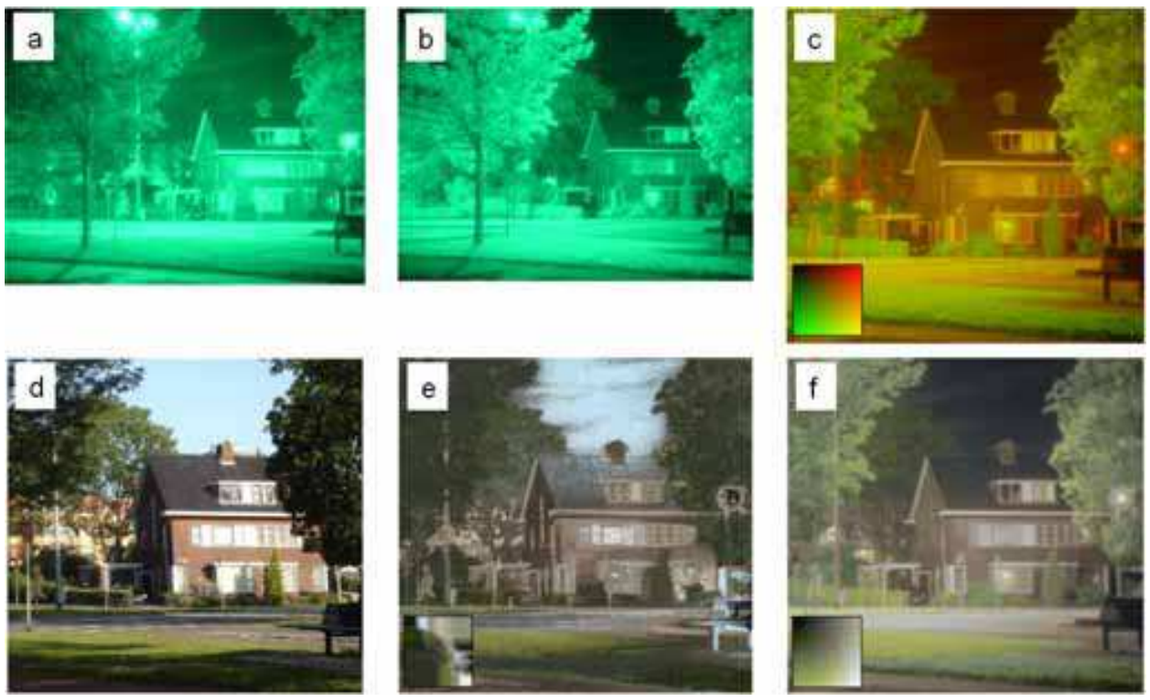

Fig. 8. Visual (a) and near-infrared (b) images of the same scene. (c) Combined red-green false color representation of (a) and (b). (d) Daytime reference color image. (e) Result of straightforward application of the sample-based transform method. (f) Result after smoothing and linearising the color lookup table.

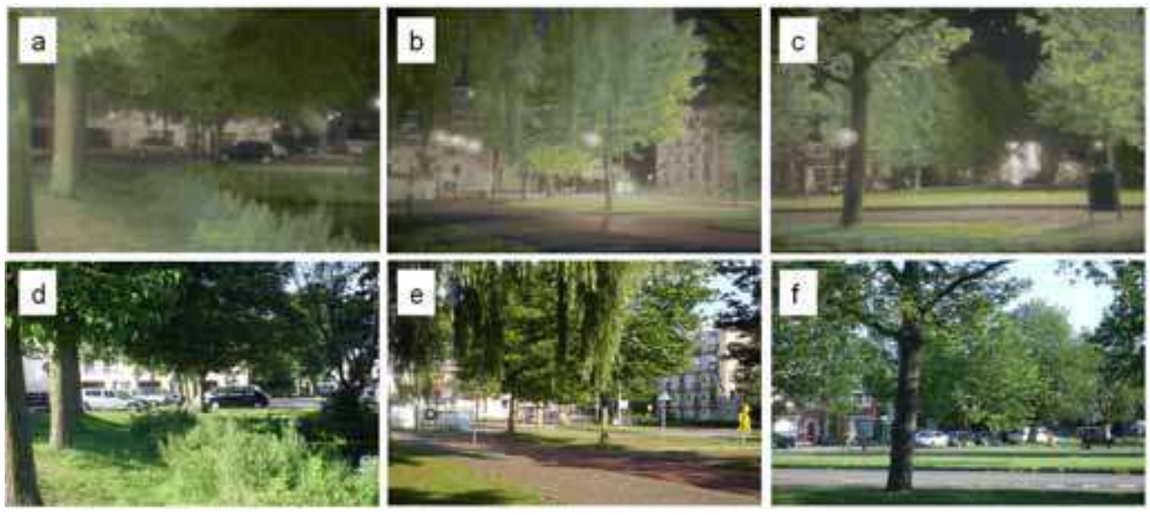

Fig. 9. (a-c) Results of applying the coloring scheme from Fig. 8f to different multi-band sensor images. (d-f) Daylight color images corresponding to (a-c).

mapping scheme should then be selected to colorize the night-time images. The color transformation consists of *(1)* creating a false-color image (e.g. an RG-image, see Fig. 6e), *(2)* converting this image into an index image using the RG-color table, and *(3)* replacing the

color lookup table with its daytime equivalent (RGB-color table, see Fig. 6d, right). The whole transformation is defined by the two color lookup tables (the RG-color table and the RGB color table). The software implementation can be very fast.

Different environments require different color mapping schemes to obtain a correct color representation. The sample images used to derive the color mapping scheme should reflect the statistics of the environment in which the mapping will be deployed.

In practice the ratio between the sensor outputs is characteristic for different materials. This becomes apparent when one inspects the color map images (e.g. Fig. 6d, right side) corresponding to the optimal color mapping of different reference and test images. In those images the hue varies little along straight lines through the top-left corner (lines for which the ratio between the two sensor outputs has a constant value). This feature can be used when deriving a color mapping from a limited number of samples. Also, the color mapping (e.g. Fig. 6d, right side) can be expected to be smooth, i.e. from point to point the color variations will be smooth. When a smooth color mapping scheme is used more subtle differences between sensor outputs will become visible.

Because the sample-based color mapping is highly specific it can effectively be used to highlight interesting image details which may otherwise go unnoticed. Camouflaged targets (e.g. persons or vehicles in military colors) are usually indistinguishable from their local background in naturally colored images. As a result, they will also have low color contrast when a natural color mapping is applied to multi-band nighttime imagery. An example of this effect is shown in Fig. 10, which presents an intensified image (Fig. 10a) and a thermal infrared (8-12 μm) image (Fig. 10b) of a person wearing a military battle dress with a camouflage pattern in a rural background. Fig. 10c shows the two-band false color image that is constructed by mapping the images from Fig. 10 (a) and (b) to respectively the R and G channels of an RGB color image (the B channel was set to zero). Fig. 10d shows the full color daytime reference image (a standard digital color photograph). Using the sample-based method we derived the color transformation that results in an optimal match between the colors in the reference image (Fig. 10d) and the multi-band sensor values (Fig. 10c). The color transformation for all sensor combinations is represented by the insets of Fig. 10c and Fig. 10e, while Fig. 10e shows the result of the color mapping. Note that the colors in the colorized multi-band image (Fig. 10e) closely match the colors in the reference image (Fig. 10d). However, since the person wears clothing in camouflage colors, he is also camouflaged in the colorized nighttime image. Although the person is clearly visible in the thermal image (Fig. 10b) he can hardly be detected in the colorized nighttime image. To make the person more salient in the colorized night-time image a color transformation can be used that depicts hot items (which usually are potential targets like vehicles or living beings) in red. For this purpose we created an alternative color mapping by manipulating the inset of Fig. 10e. The resulting lookup table is depicted in the inset of Fig. 10f. Fig. 10f shows the result of the application of this color transformation to the false color two-band nighttime image in Fig. 10c. Hot items now appear in red while the (relatively cold) background is still depicted in its natural colors. In this image representation, the naturally colored background provides the context and potential targets are highlighted by their color contrast. This color mapping may be useful for applications like surveillance and navigation, since these tasks require a correct perception of the background (terrain) for situational awareness in combination with optimal detection of targets and obstacles.

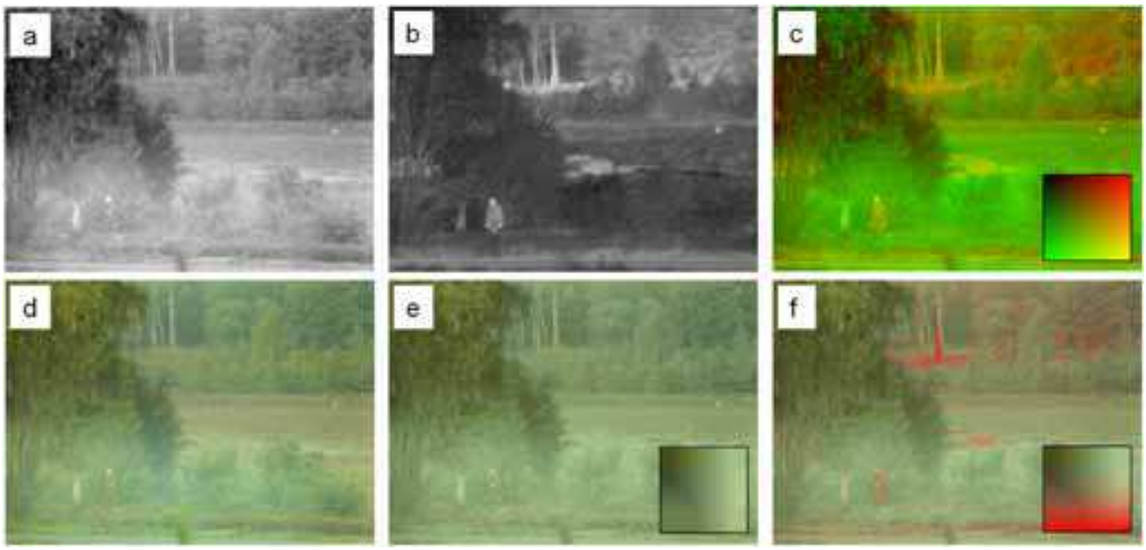

Fig. 10. Result of the application of a natural color mapping to a two-band nighttime image. (a) Intensified visual image and (b) thermal (8-12 μm) image of a rural scene with a person standing in the foreground. (c) Two-band false color image obtained by mapping (a) and (b) to respectively the G and R channels of an RGB color image (the B channel was set to zero). (d) A daylight color picture of the same scene. (e) Result of the application of the color mapping defined by inset to (c). (f) Result of the application of the color mapping defined by the inset to (c).

3. Implementation

In the next sections we describe three prototype portable dual band real-time hardware implementations of nighttime image acquisition systems that deploy the lookup-table color transform method. The first system creates a color nightvision image by fusing the visual and near-infrared bands of two identical image intensifiers. The second system presents a color fused image of the signals of an image intensifier and a longwave infrared thermal camera. The third system produces a three-band nighttime image by combining the visual and near-infrared bands of two identical image intensifiers with a longwave infrared image.

3.1 The Gecko system: combination of visual and near-infrared

The Gecko sensor module provides co-axially registered visual and NIR images. This system is named after nocturnal geckos that still have color vision at very dim light levels (Roth & Kelber, 2006). The Gecko system includes 2 image intensifiers, 2 compact EO cameras, a heat reflecting (hot) mirror, and a near-infrared reflecting mirror (Fig. 11). The image intensifiers are two GEN III type Mini N/SEAS monocular night vision goggles (NVGs) from International Technologies Lasers Ltd (ITL). They provide a 1x magnification, and have a circular field-of-view (FOV) with a diameter of 40 deg, corresponding to about 2000 pixels. They are sensitive in the visual and near infrared part of the spectrum. Both image intensifiers are placed side by side. A distinctive characteristic of the construction of our acquisition unit is the hardware registration of both NVG images. A co-aligned view is achieved through the use of a hot mirror in combination with a NIR reflecting mirror (Fig.

11a). The hot mirror is an Edmund Optics (www.edmundoptics.com) NT43-958 3.3 mm thick mirror, intended for an angle of incidence of 45°, with a multi-layer dielectric coating that reflects infrared radiation (heat), while allowing visible light to pass through. The NIR radiation is reflected by a Melles Griot 01 MFG 011 mirror (www.mellesgriot.com) that is covered with a protected aluminum coating, which has an average reflectance greater than 87% over the spectral range from 400 to 800 nm (fig. 3b). As shown in Fig. 11a, the hot mirror acts as a dichroic beam splitter, transmitting the visual part of the incoming radiation to the upper NVG, while reflecting the NIR part via the NIR reflecting mirror into the lower NVG. The image from each NVG is registered by a PixeLINK PL-A741 MV FireWire 1.3 megapixel monochrome camera with a 2/3" CMOS detector with a resolution of 1280 x 1024 pixels (www.pixelink.com). Both cameras are equipped with a 16 mm Pentax C1614A C-mount lens, yielding a horizontal FOV of 30º72'T. They operate either at 33 fps at an image size of 1k x 1k, or 105 fps at 640 x 480 pixels. After processing the two-band Gecko signals on a notebook computer the resulting colorized imagery is displayed on the screen of the notebook computer, or, alternatively, on miniature head-mounted displays

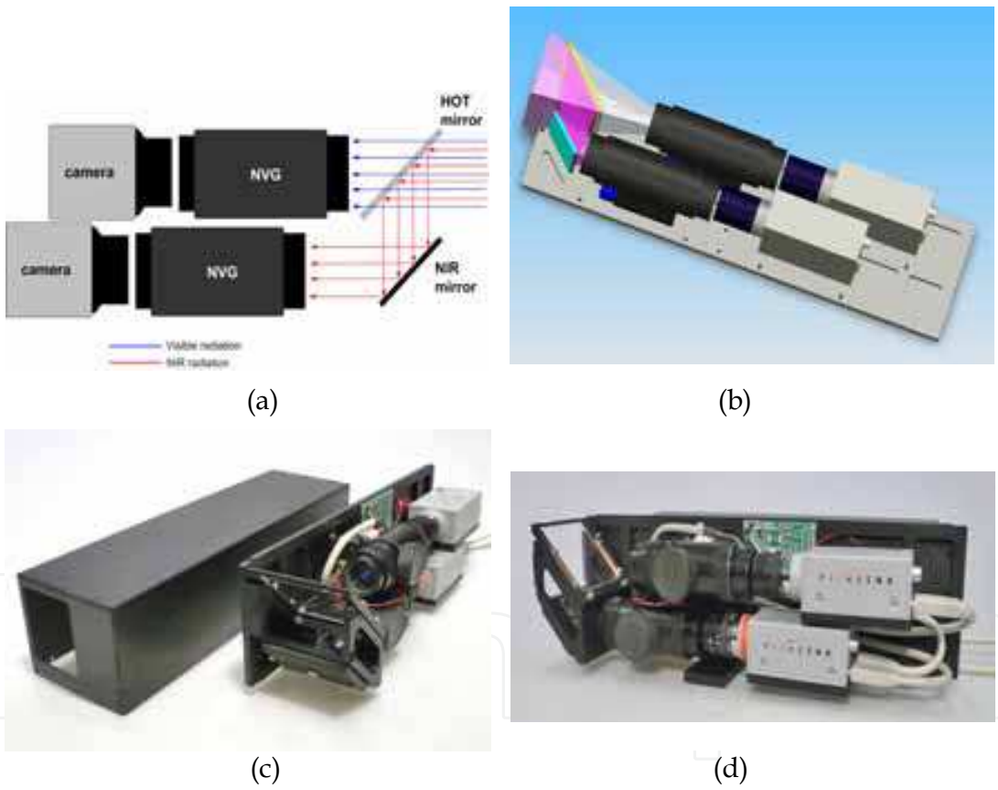

Fig. 11. The dual band Gecko system. (a) Schematic representation. (b) 3D view of the system design. (c) Front view of the system and its casing. (d) Side view.

The incoming video stream can also be stored on the hard disk of the notebook computer. The system as a whole is portable and can therefore be used to assess the benefits of color fusion in realistic surveillance and navigation scenarios.

Fig. 12d shows the Gecko image of a park scene after the application of our new color remapping technique (in this case swapping the color table of Fig. 12c by that of Fig. 12d). This multiband nightvision image closely resembles the corresponding daytime photograph

(Fig. 12e). Note that it is much easier to distinguish different materials and objects in Fig. 12d, compared to each of the individual bands (a,b) or an RG false color fused image (c).

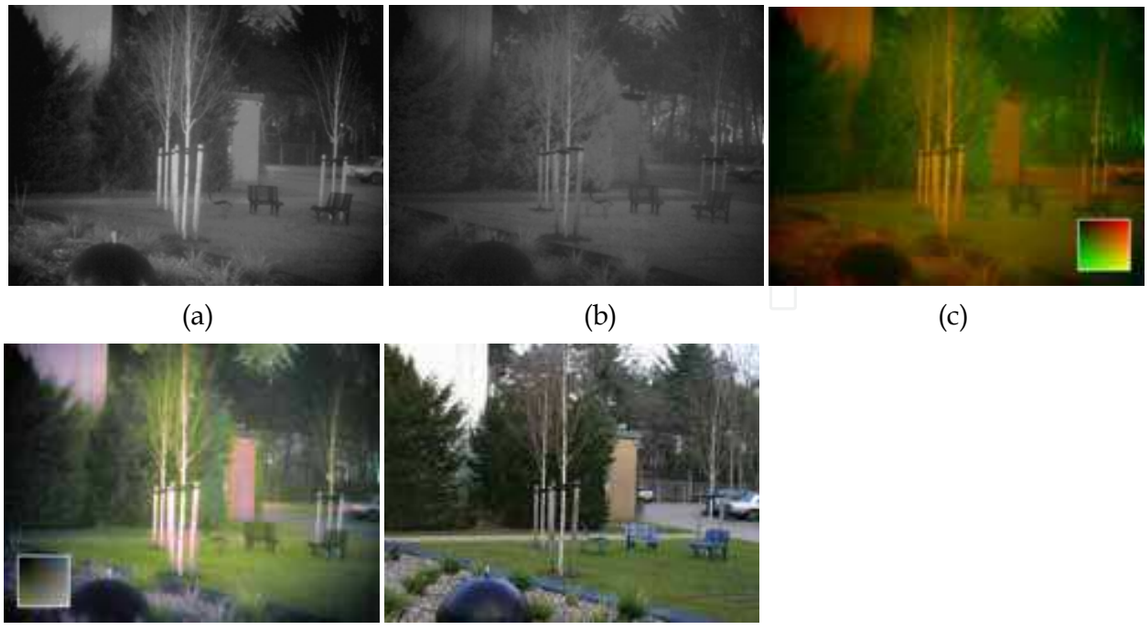

(a) (b) (c)

(d) (e)

Fig. 12. (a) Visual (wavelengths below 700 nm) and (b) NIR (wavelengths above 700 nm) images of a park scene. (c) False color combination with the Visual image (a) in the Red and the NIR image (b) in the Green channel of an RGB color image. (d) The result of our color remapping technique. (e) A daytime color photograph of the same scene. The square insets in images (c) and (d) represent their corresponding color tables.

Fig. 13d shows the Gecko image of a road scene after the application of our new color remapping technique (in this case swapping the color table of Fig. 13c by that of Fig. 13d). This multiband nightvision image closely resembles the corresponding daytime photograph (Fig. 13f). For comparison we also show the standard intensified (NVG) image in Fig. 13e. Note that it is much easier to distinguish the borders of the road in Fig. 13d, compared to a standard NVG image Fig. 13e.

3.2 The Viper system: combination of visual and longwave infrared

The Viper sensor module provides co-axially registered visual and longwave infrared (LWIR) or thermal images. This system is named after a species of snake that fuses in its optic tectum the visual images from its eyes with thermal images from infrared sensitive organs that function like pinhole cameras (Newman & Hartline, 1982). The Viper sensor module includes a compact infrared microbolometer, a digital image intensifier, and 2 hot mirrors (Fig. 14). The FLIR Systems ThermoVision A10 infrared microbolometer has a 160 x 128 pixel focal plane array, and a spectral sensitivity range of 7.5 – 13μm, which is the range of most interest for outdoor applications. It is equipped with an 11mm (f/1.6) lens providing a 40° x 30° wide angle view. The ThermoVision A10 delivers wide dynamic range (14-bit) analog video output at 30 Hz (for RS-170) or at 25 Hz (for CCIR). It has a NETD of <85 mK. The Intevac NightVista E1100 digital image intensifier has a 1/2" sensor with a spectral

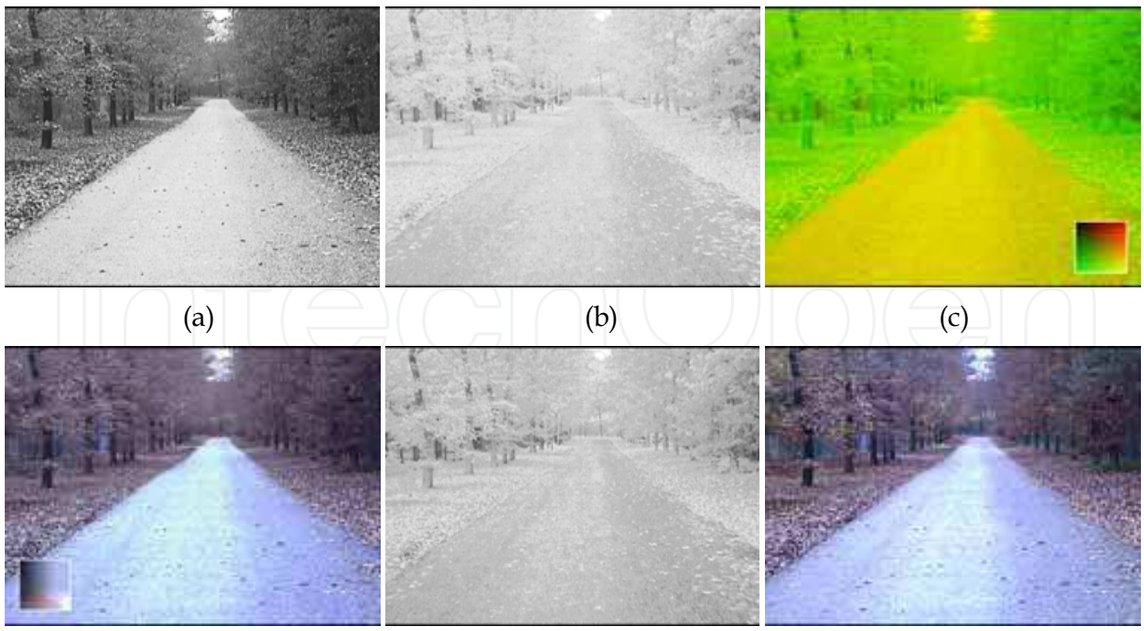

(a) (b) (c)

(d) (e) (f)

Fig. 13. (a) Visual (wavelengths below 700 nm) and (b) NIR (wavelengths above 700 nm) images of a road scene. (c) False color combination with the Visual image (a) in the Red and the NIR image (b) in the Green channel of an RGB color image. (d) The result of our color remapping technique. (e) Standard NVG image (= a+b). (f) A daytime color photograph of the same scene. The square insets in images (c) and (d) represent their corresponding color tables.

response range 400-900 nm, and delivers RS-170 VGA resolution (640x480) video signal output at 30 fps. It is equipped with an 8.5 mm C-mount Pentax C815B lens, yielding a view of 42.09^{o} horizontally. The intensified and thermal images are co-aligned through the use of a pair of hot mirrors (Fig. 14a). The first mirror is an Edmund Optics (www.edmundoptics.com) NT43-958 3.3 mm thick mirror, intended for an angle of incidence of 45°, with a multi-layer dielectric coating that reflects infrared radiation (heat), while allowing visible light to pass through. The second mirror is a gold coated borosilicate crown optical glass plate (type BK7, CRYSTECH Inc, www.crystech.com), with a reflection coefficient larger than 99.8%.

The analog video signals of the A10 infrared microbolometer and the Intevac digital image intensifier are both converted into 8 bits digital signals by means of a DFG/1394-1e DFG/1394-1e Video-to-FireWire converter (www.theimagingsource.com) that was inserted in a Dell Inspiron 9300 notebook computer. As a result of the co-axial image registration parallax problems are eliminated and only minimal spatial alignment and image stretching (to correct for the slight difference in FOV size of both cameras) is needed before image/video exploitation. The resulting registered images are combined into an RGB format for further processing (the B channel is set to zero). The previously described color mapping is implemented as a color lookup table transform.

After processing the two-band Viper signals on a notebook computer the resulting colorized imagery is displayed on the screen of the notebook computer, or, alternatively, on miniature head-mounted displays The incoming video stream can also be stored on the hard disk of

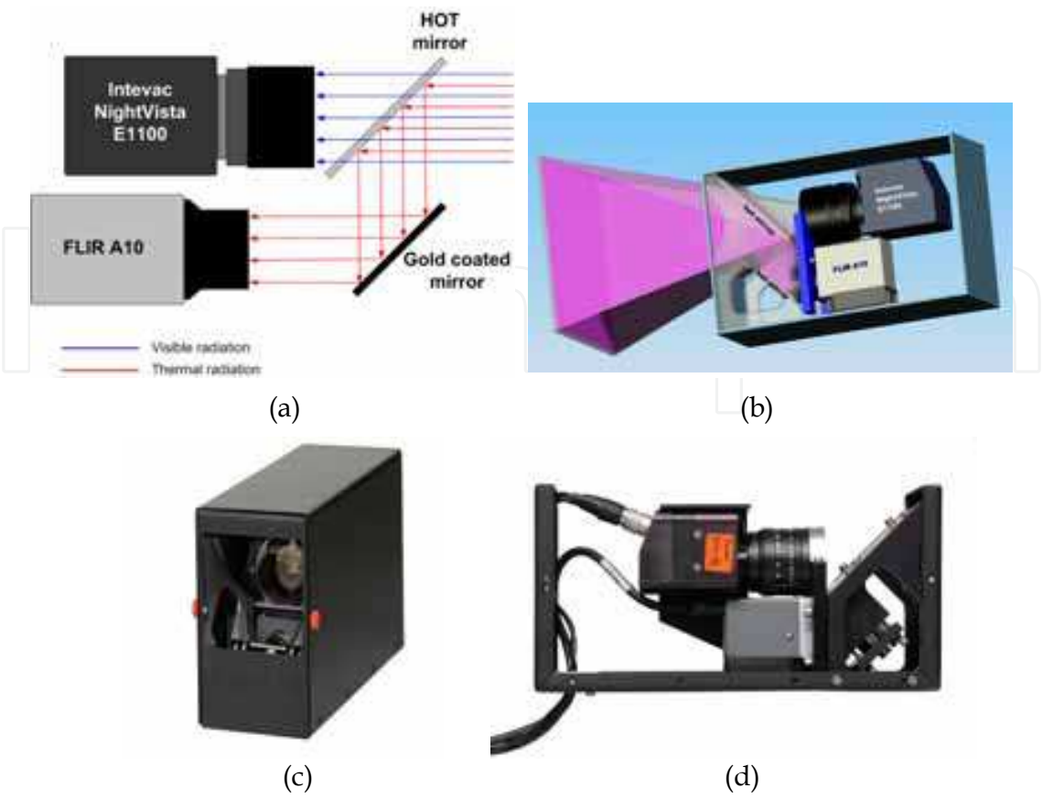

Fig. 14. The dual band Viper system. (a) Schematic representation. (b) 3D view of the system design. (c) Front view of the system and its casing. (d) Side view.

the notebook computer. The system as a whole is portable and can therefore be used to assess the benefits of color fusion in realistic surveillance and navigation scenarios.
Fig. 15d and e show the Viper image of a park scene after the application of our new color remapping technique (in this case swapping the color table of Fig. 15c by that of Fig. 15d and Fig. 15e). The results are shown for 2 different mappings. Note that objects in the scene, particularly the person, are much easier to distinguish in these color remapped images compared to each of the individual bands (Fig. 15a,b) or an RG false color fused image (Fig. 15c).
Fig. 16d shows the Viper image of a battle scene after the application of our new color remapping technique (in this case swapping the color table of c by that of d). Note that both the soldier and the smoke screen are clearly visible and represented in their correct (true) colors in the recolored Viper image (d), whereas only one of these can be seen in the individual bands (a,b).

3.3 The TRICLOBS system: combination of visual, near-infrared and longwave infrared

The TRICLOBS (TRI-band Color Low-light OBServation) system combines a three-band nightvision sensor suite, consisting of two digital image intensifiers and a thermal (LWIR) camera, in combination with a 3D digital position information system. The night vision sensor suite is sensitive in the visual (400-700 nm), the near-infrared (700-1000 nm) and the longwave infrared (8-14 μm) bands of the electromagnetic spectrum. The optical axes of all cameras are aligned.

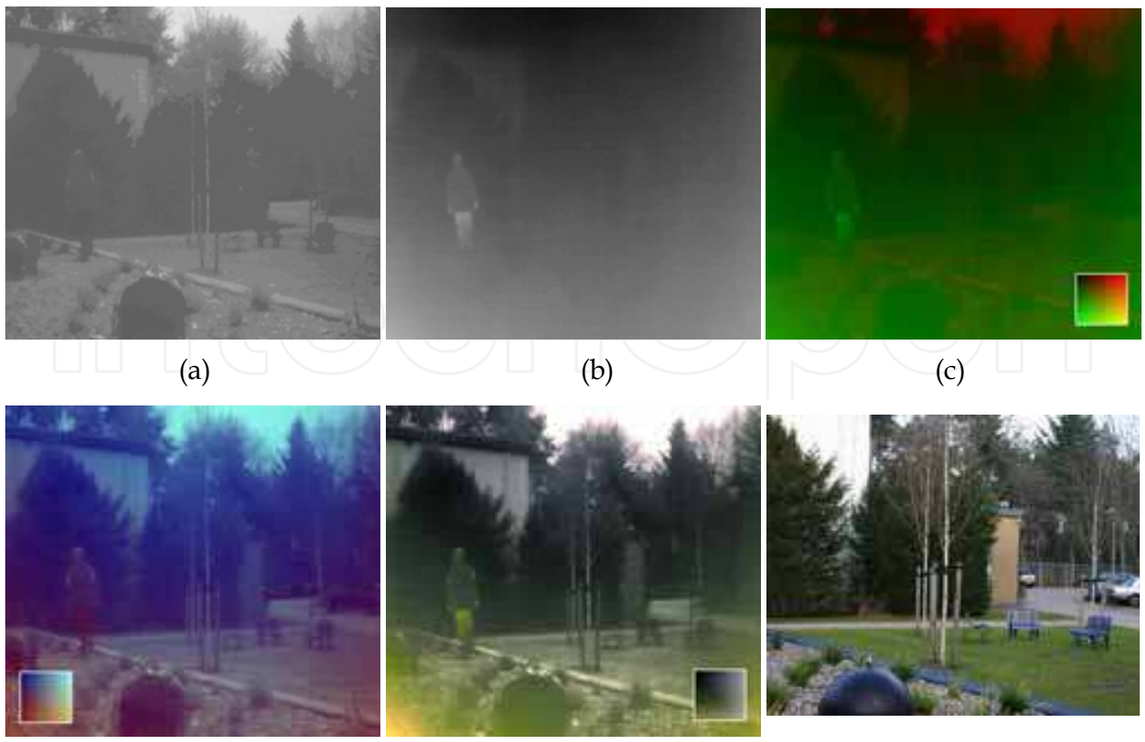

(a) (b) (c)

(d) (e) (f)

Fig. 15. (a) Visual intensified and (b) LWIR (8-12 μm) images of a park scene. (c) False color combination with the Visual image (a) in the Red and the LWIR image (b) in the Green channel of an RGB color image. (d-e) The result of our color remapping technique for two different lookup tables. (f) A daytime color photograph of the same scene. The square insets in images (c,d,e) represent their corresponding color tables.

Fig. 17 shows a schematic representation of the layout of the sensor suite and the beam splitters that are deployed to direct the appropriate band of the incoming radiation to each of the 3 individual sensors. The incoming radiation is first split into a longwave (thermal) and a visual+NIR part by a heat reflecting (hot) mirror (a custom made Melles Griot dichroic beam splitter consisting of Schott N-BK7 Borosilicate Crown glass with an Indium Tin Oxide coating, with a reflection R > 85%). The longwave part of the spectrum is reflected into the lens of the thermal camera, while the visual+NIR light is transmitted to a combination of two digital image intensifiers that are mounted under an angle of 90 degrees. Next, a near-infrared reflecting mirror (45 deg angle of incidence, Borofloat glass, type Edmund Optics B43-958, 101x127x3.3 mm, see: www.edmundoptics.com) is used to separate the incoming light, by transmitting the visual (400–700nm) and reflecting the NIR part (700–900nm), such that one image intensifier registers the visual part and the other one only detects the NIR part of the incoming radiation. The sensor geometry is such that the optical axes of all cameras are aligned.

The two image intensifiers are high resolution (1280x960) Photonis PP3000U Intensified Camera Units (ICUs: www.photonis.com). The ICU is a low light level, intensified CMOS camera. It has a 2/3" CMOS sensor with a spectral response range of 400-900 nm, and delivers both a PAL or NTSC composite video signal output (ITU-R BT.656-4, 640x480

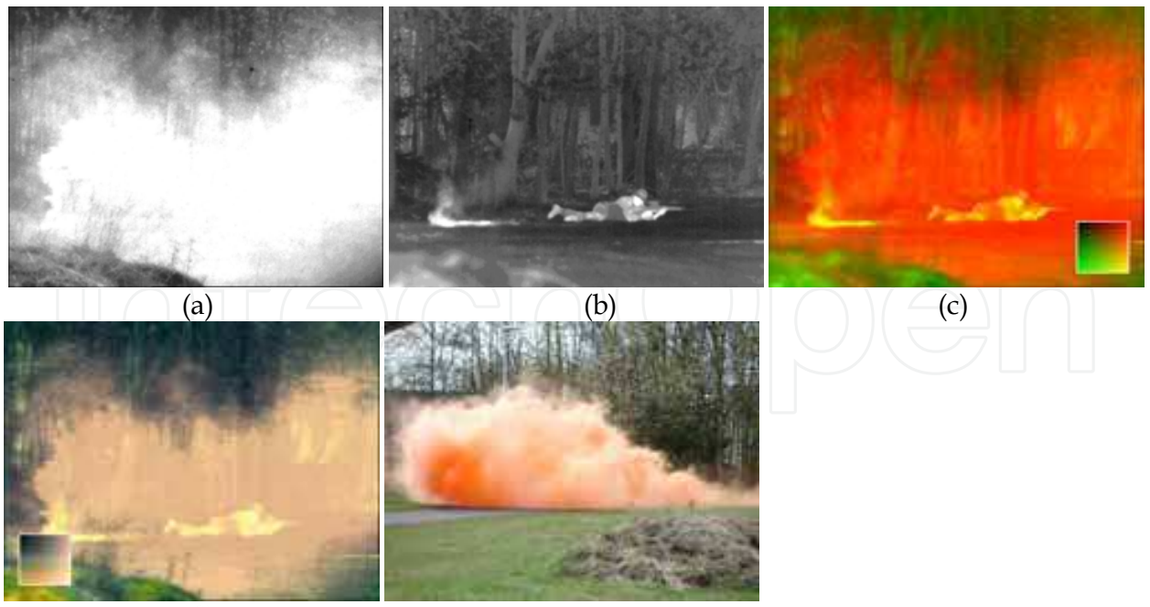

Fig. 16. (a) Visual intensified and (b) LWIR (8-12 μm) images of a battle scene. (c) False color combination with the Visual image (a) in the Red and the LWIR image (b) in the Green channel of an RGB color image. (d) The result of our color remapping technique. (e) A daytime color photograph of the same scene. The square insets in images (c,d) represent their corresponding color tables.

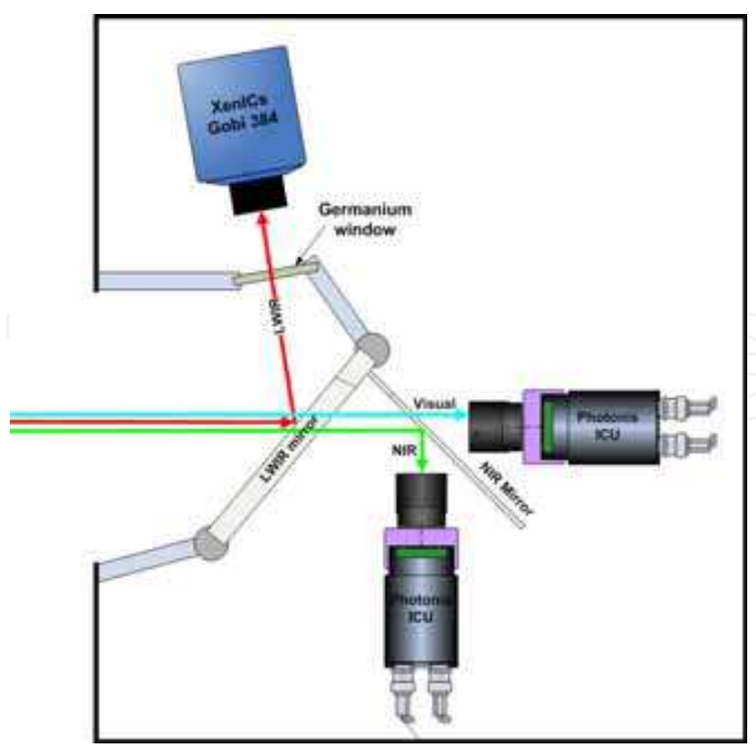

Fig. 17. Layout of the sensors and filters of the TRICLOBS sensor suite.

pixels), and an SDI – LVDS 270 Mbits/s signal. Both ICU's are equipped with Pentax C2514M CCTV lenses, with a minimal focal length of 25mm and a lens aperture of F/1.4, resulting in a FOV of 30.7º x 24.8º. The thermal camera is a XenICs Gobi 384 uncooled a-Si infrared microbolometer (www.xenics.com). It has a 384 x 288 pixel focal plane array, and a spectral sensitivity range of 8–14μm, which is the range of most interest for outdoor applications. It is equipped with an Ophir supIR18mm F/1 lens (www.ophiropt.com) providing a 29.9° x 22.6° wide angle view. The Gobi 384 has a 16-bit Ethernet and CameraLink interface.
The sensors are mounted a common metal frame, which is placed in an enclosed housing. All signal processing is done on a standard laptop. The system is mounted on a mobile all-terrain platform Fig. 18.

(a)

(b)

(c)

Fig. 18. The TRICLOBS sensor suite. (a) Top view, (b) inside , and (c) the sensor suite mounted on a mobile all-terrain platform.

4. Evaluation study

As noted before, natural color mapping schemes are not suitable for all purposes. A typical example is the task of finding a camouflaged soldier in a field, using a two-band nightvision system sensitive to the visual and thermal part of the electromagnetic spectrum. When the false color representation of the nightvision image optimally agrees with the daytime appearance of the scene, the soldier will be camouflaged, which is obviously not very helpful for the task at hand. In such cases a color mapping scheme should be deployed that represents the objects of interest with higher color contrast while still providing a color

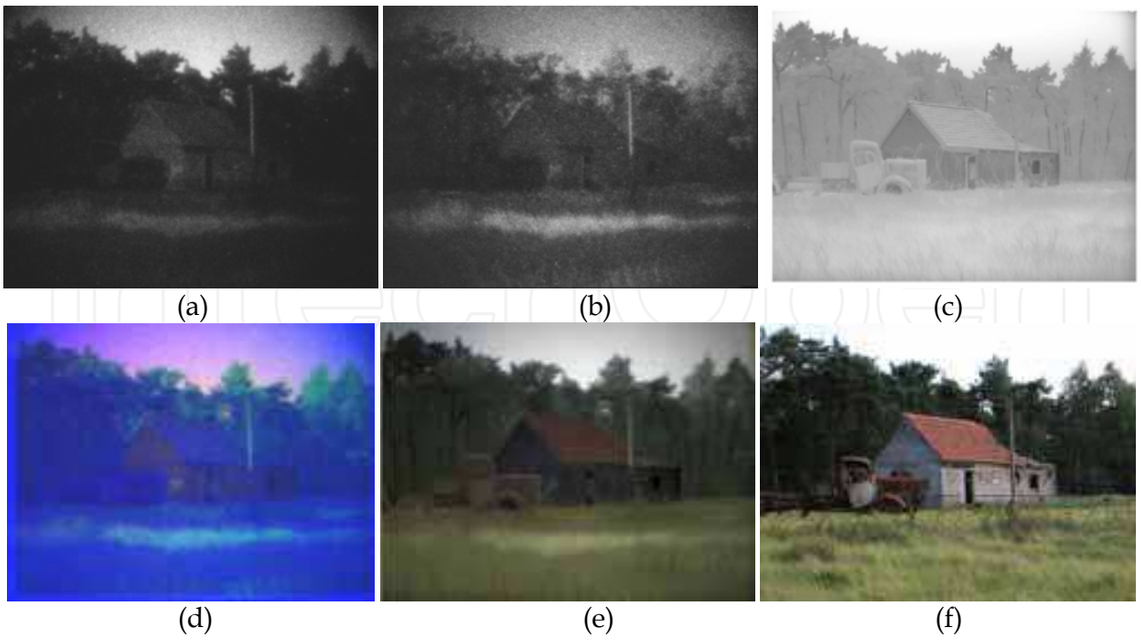

(a) (b) (c)

(d) (e) (f)

Fig. 19. Nighttime scene showing a house with a person in front, a truck and some trees. (a) Visual, (b) NIR and (c) LWIR input signals. (d) False color image obtained by mapping the three bands to respectively the R, G, and B channels. (e) Result of color remapping applied to (d). (f) Corresponding daytime image.

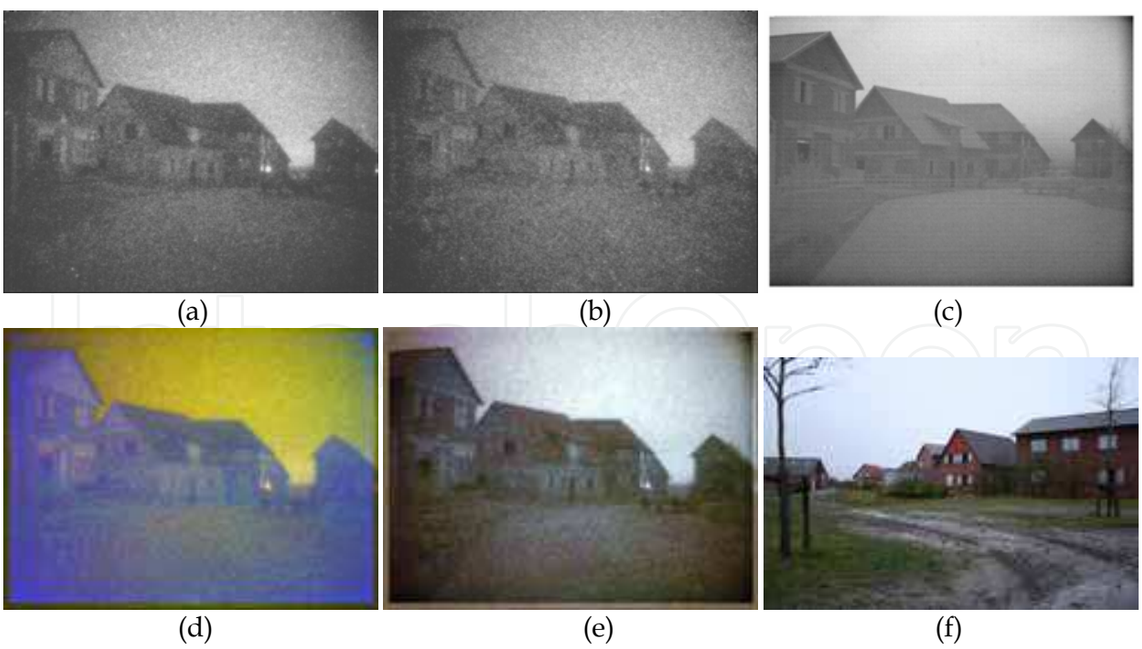

(a) (b) (c)

(d) (e) (f)

Fig. 20. Nighttime scene showing some houses, grass and a road. (a) Visual, (b) NIR and (c) LWIR input signals. (d) False color image obtained by mapping the three bands to respectively the R, G, and B channels. (e) Result of color remapping applied to (d). (f) Corresponding daytime image.

setting for the rest of the scene which is intuitively correct. We designed such a color scheme, which is targeted at optimizing the detection of (camouflaged) targets that do not contain chlorophyll, while still providing reasonably natural colors.
The dual-band Gecko system was used to register optically aligned visual (wavelengths shorter than 700 nm) and near infrared (wavelengths longer than 700 nm) images. For comparison we also created a standard intensified image of each scene containing both bands, since this is the type of image typically provided by standard night vision goggles. The visual band is represented by the Red channel of an RGB-image and the near-infrared band by the Green channel, to create a red-green representation of the dual-band sensor image (Fig. 21d). Next, for each combination of sensor outputs (represented by a shade of red, green, yellow; see inset of Fig. 21d) a color was chosen to display this sensor output. This process can be implemented by transforming the red-green image (Fig. 21d) into an indexed image in which each pixel value refers to the entry of a color lookup table. When a color lookup table is used with different colors, the colors in the indexed image are

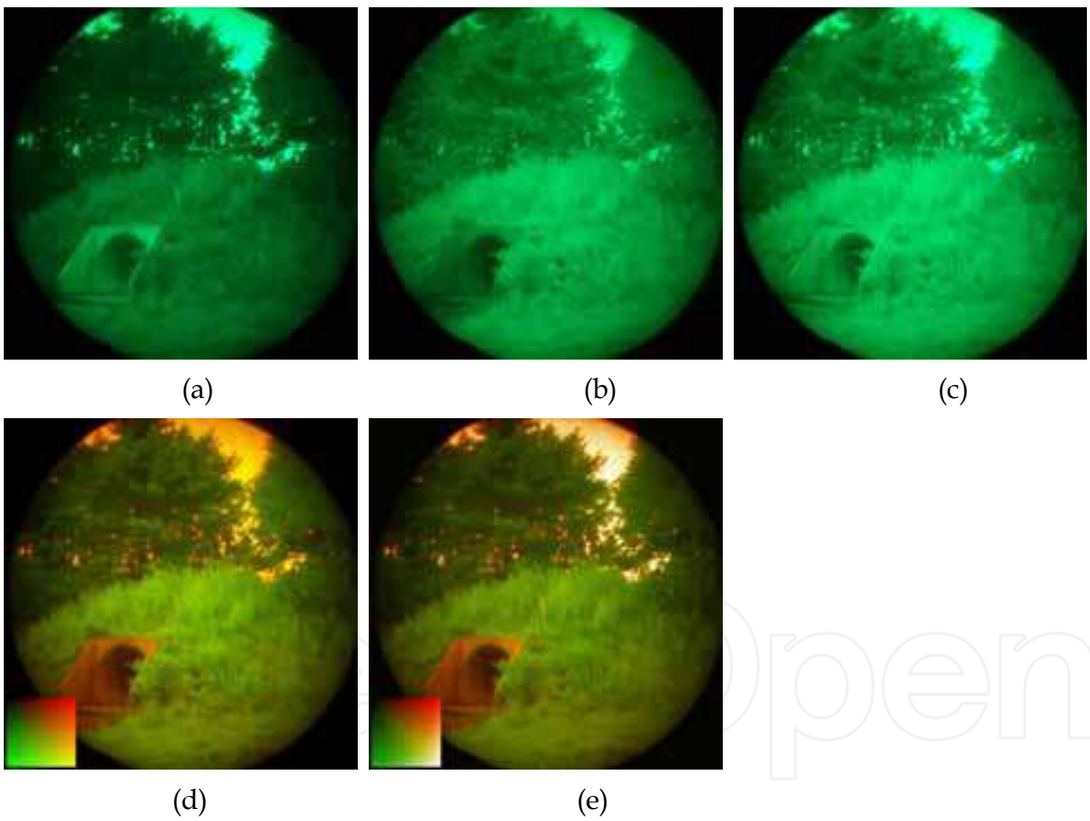

(a) (b) (c)

(d) (e)

Fig. 21. Lookup table based color remapping applied to a dual-band visual (a) and near-infrared (b) Gecko image. (c) A regular intensified image representation for comparison (e.g. a standard night vision goggle image). (d) A red-green false color representation of the dual-band image with the visual band assigned to the Red and near-infrared band assigned to the Green channel of an RGB display. The inset in (d) shows all possible dual-band outputs as shades of red (large response in band 1, small in band 2), green (small response in band 1, large in band 2) and yellow (large responses in both bands). (e) The result of the color transformation. The inset shows how the colors in the inset of (d) are transformed.

automatically transformed into other colors, in a way that all pixels with the same index will result in the same color. The method is described in detail elsewhere (Hogervorst & Toet, 2008a; Hogervorst & Toet, 2010). We tried several color transformations in our search for a color scheme that results in optimal detection of targets while preserving the natural appearance of images. The best color transformation we found for our purposes looks similar to the red-green representation, with a few modifications.

The inset of Fig. 21e shows the colors assigned to all dual-band outputs (represented by the inset of Fig. 21d) by the chosen color scheme. This color scheme emphasizes the distinction between objects containing chlorophyll (the background plants) and objects containing no chlorophyll (e.g. our targets; notable from the sharp transition between green and red at the diagonal). The Gecko sensor system separates the incoming light in a part with wavelength below 700nm and one with wavelengths above 700 nm. Since chlorophyll shows a steep rise around 700nm, this dual-band NVG system is especially suited for discriminating materials containing chlorophyll from materials containing no chlorophyll. Elements containing chlorophyll (e.g. plants) are displayed in green (i.e. in their natural color), while objects without chlorophyll are displayed in the perceptually opposite color red. To further increase the naturalness, elements with high output in both channels are displayed in white (bottom right corner of the inset of Fig. 21e). The result of our color fusion method is shown in Fig. 21e.

We evaluated the abovementioned color mapping in a target detection paradigm. We registered both nighttime dual-band (visual and near-infrared) Gecko images and daytime full color digital photographs of a scene containing grass and trees, with and without targets present. Performance for detecting targets was established for imagery of the dual-band fusion system, each of the individual NVG-bands (visual and NIR), standard NVG and daytime images (taken with a visual camera). The visual angle and display area of the daytime images was matched to that of the nighttime images.

The targets were green (Fig. 22a) and blue (Fig. 22b) foam insulation tubes. The reflectance of the tubes was such the green tubes were mostly undetectable in a standard intensified image representation and in the near infrared band (see Fig. 21), but detectable (as a bright object) in the visible band (see Fig. 21). In contrast, the blue tubes were often undetectable in the visual band while being detectable (as a dark object) in the near infrared band and in regular intensified image (see Fig. 23).

(a) (b)

Fig. 22. The green target (a) and the blue target (b) situated in a background with grass and trees.

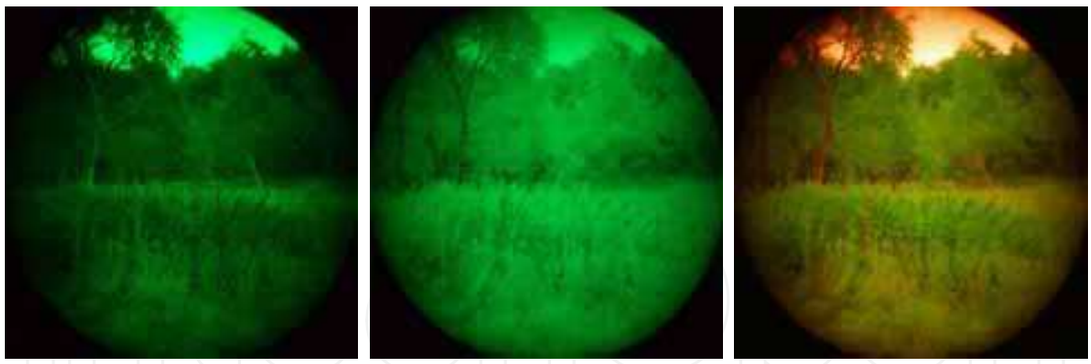

(a) (b) (c)

Fig. 23. Visual (a), near-infrared (b) and the color fused dual-band image (c) for a scene including a blue target. The target is visible in the near-infrared band as a dark tube. The dual-band image shows the target as a reddish object.

We recorded whether the subjects detected the targets when present (Hits and Misses) and whether they judged there to be a target when no target was present (False Alarms and Correct Rejections). We also recorded the response times. Since no False Alarms occurred in this experiment (i.e. the False-Alarm rate was zero), observer performance is fully characterized by the Hit-rate, i.e. the fraction of targets that was detected (ph = #Hits / (#Hits + #Misses)). Observer performance was measured for 5 different image modalities:

1. Daytime: full color daylight images (taken with a standard digital daytime camera),
2. II: grayscale intensified images, combining both visual and near-infrared
3. VIS: grayscale intensified images representing only the visual part of the spectrum,
4. NIR: grayscale intensified images representing only the near-infrared part of the spectrum,
5. FC: false color images resulting from the natural color remapping method.

For each image modality we used 56 images without a target, 26 with a green target, and 26 with a blue target. Seven subjects participated in the experiment. Each subject participated in 5 sessions in which the stimuli of each condition were shown separately. Each subject started the session with the Daylight condition to get acquainted with the procedure, the scene and the targets. The order of the remaining 4 conditions was randomized across subjects to compensate for possible training effects. The images were shown on a PC monitor with a resolution of 1600x1200 pixels (Fig. 22 gives a realistic representation of the display content).

Each experimental session started by explaining the purpose of the experiment and by showing some example stimuli of each condition. Each trial started by presenting an image. The subjects were required to decide as quickly as possible whether a target was present or not. As soon as this decision was taken the subjects clicked the mouse button. Next, the image disappeared and was replaced by a low resolution equivalent of the image, consisting of 20x15 uniformly colored squares (to prevent subjects from searching for the target after responding). We registered the time between onset of the stimulus and detection (the response time). The subject then indicated the target location or clicked on an area outside the image labeled “no target found”. When the subject did not respond within 8 seconds the trial ended automatically. The indicated target location was used to check whether the subject had indeed detected the target or had seen a false target. Responses outside an

ellipse with horizontal diameter of 162 and vertical diameter of 386 pixels centered on the vertically elongated target were treated as incorrect.

Fig. 24 shows the fraction of hits (hit-rate) for the various sensor conditions and target colors. Shown are the average hit-rates over subjects. Not surprisingly, performance is highest in the Daytime condition. As expected (see Fig. 21 and Fig. 23), performance for detecting the green targets is high in the visual (VIS) condition and low in the image intensified (II) and near-infrared (NIR) sensor conditions. Performance for detecting the blue targets is somewhat poorer in the single-band conditions. These targets can be detected in the NIR condition (reasonably well) and in the II condition (poorly), while they are hardly detected in the VIS condition. Detection performance for both targets is high with the false-color dual-band sensor. Optimal fusion results in performance that equals maximum performance in the individual bands. The hit-rate for the green targets is somewhat lower for the dual-band than for the visual condition. But the hit-rate for the blue targets is somewhat higher for dual-band than for NIR condition. The average hit-rate of the false color dual band sensor (0.75) is not significantly different from the average of the hit-rate for green in VIS and the hit-rate for blue in NIR (0.78). This means that this fusion scheme is (close to) optimal. The results also show that the performance with the standard intensified imagery is clearly much worse than with the false-color dual-band NVG system.

Fig. 25 shows the response times of the trials containing a target (shown are the geometric means over the response times, i.e. the exponent of the average log response times) for all conditions for the hits and misses. Note that the hits for the NIR and II modalities correspond primarily to the trials containing blue targets; the hits for the Visual modality correspond primarily to the trials containing green targets. The response times for the false color dual-band condition are comparable, but slightly larger than in the single-band Visual

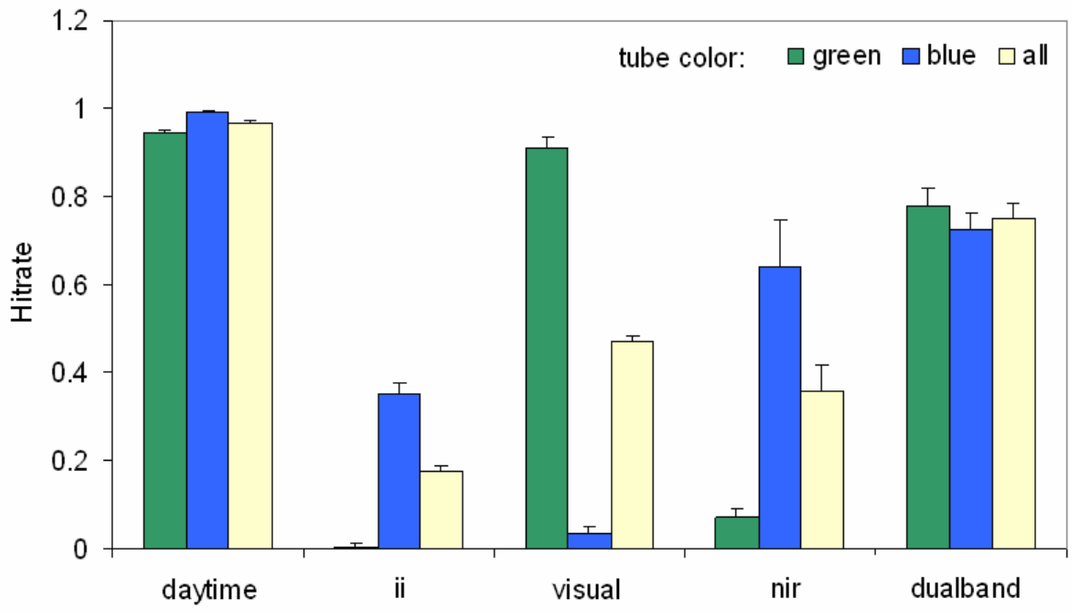

Fig. 24. Average (over all subjects) hit-rate (fraction of hits) for each of the 5 different image modalities and the 2 target colors, including the overall hit-rate ("all"). The error bars represent standard errors in the mean derived from the variance between subjects.

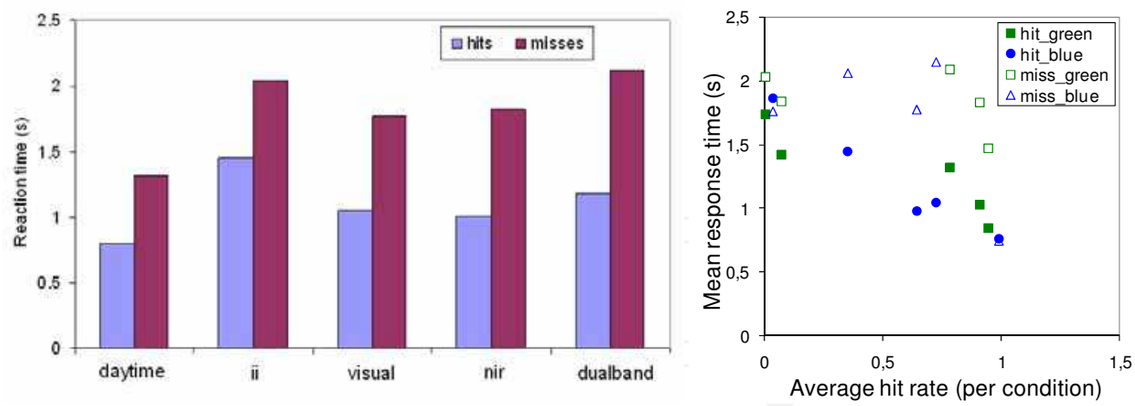

(a) (b)

Fig. 25. (a) The geometric mean (i.e. averaged in log) response times for the various image modalities, separated for hits and misses. (b) Relationship between the hit-rate for each image modality and the (geometric) mean response times for hits and misses for the two target colors.

and NIR conditions. This may be due to the fact that in this condition subjects had to attend to two types of targets, while in the single band conditions only one of the target colors was apparent.

It turns out that the response times for missed targets are comparable to the response times for stimuli in which no target is present. The average response times for missed targets do not correlate with the hit-rates (see Fig. 25b). In contrast, the average response times for hits is highly correlated with the hit-rate ($r = -0.90$, $p < 0.01$, see Fig. 25b). This indicates that when targets are more easily detected, the hit-rate goes up and the response time goes down.

Summarizing, the results show that performance of the false color dual-band system is just as good as the maximum performance that can be attained using either of its individual bands (visual and near-infrared). While the green targets can well be detected with the visual band of the system alone, the blue targets are mostly missed when subjects have to rely on this band alone. In contrast, the blue targets can well be detected with the near-infrared band, but the green targets are then largely missed in this modality. With the false color dual-band image modality both targets can be detected. The total number of targets detected in the dual band image modality is the same as the total number of targets detected in the visual and modality plus the number of targets detected in the near-infrared image modality. This indicates that the fused color representation of the two bands is (nearly) optimal from a perceptual standpoint.

5. Conclusion

In this chapter we presented three prototype portable multiband realtime night vision systems that deploy lookup table based real-time color remapping to represent nighttime imagery with a natural daylight color appearance and to enhance the detection of camouflaged targets. The systems provide respectively registered dynamic visual and near-infrared (Gecko system), visual and longwave infrared (Viper system), or visual, near-infrared and thermal images (TRICLOBS system). These co-aligned images can either be

stored on on-board harddisks, or they can be processed in real-time by a (notebook) computer. The real-time color remapping that gives the multiband signals their intuitive color appearance is implemented as a lookup table transform. The results of some laboratory experiments and preliminary field trials clearly demonstrate the benefits of these systems for surveillance, navigation and target detection tasks. The resulting false color nightvision images closely resemble daytime images (thus providing situational awareness), while thermal targets are clearly distinguishable (thus enabling target detection).
The practical value of these systems will be further evaluated in extensive field trials using realistic surveillance and navigation scenarios. Also, the systems will be used to collect a nighttime imagery in a wide range of environmental conditions and various geographical locations. This imagery will be used in laboratory observer studies and will serve as input to computational and information theoretic measures (Chen et al., 2008; Chen & Blum, 2009; Tsagaris, 2009; Tsagaris & Anastassopoulos, 2006) to assess the operational benefits of the new color mapping procedures. Further improvements of the color mapping method that will be implemented next are the optimization of color contrast (Yin et al., 2010) and image dehazing based in information from the near-infrared channels (Schaul et al., 2009).

6. Acknowledgement

Effort sponsored by the Air Force Office of Scientific Research, Air Force Material Command, USAF, under grant number FA8655-09-3095. The U.S. Government is authorized to reproduce and distribute reprints for Governmental purpose notwithstanding any copyright notation thereon.

7. References

Aguilar, M.; Fay, D.A.; Ireland, D.B.; Racamoto, J.P.; Ross, W.D. & Waxman, A.M. (1999). Field evaluations of dual-band fusion for color night vision, In: *Enhanced and Synthetic Vision 1999*, Verly, J.G. (Eds.),Vol. SPIE-3691, pp. 168-175, The International Society for Optical Engineering, Bellingham, WA.

Aguilar, M.; Fay, D.A.; Ross, W.D.; Waxman, A.M.; Ireland, D.B. & Racamoto, J.P. (1998). Real-time fusion of low-light CCD and uncooled IR imagery for color night vision, In: *Enhanced and Synthetic Vision 1998*, Verly, J.G. (Eds.),Vol. SPIE-3364, pp. 124-135, The International Society for Optical Engineering, Bellingham, WA.

Ansorge, U., Horstmann, G. & Carbone, E. (2005). Top-down contingent capture by color: evidence from RT distribution analyses in a manual choice reaction task. *Acta Psychologica*, Vol.120, No.3, 243-266.

Bandara, S.V., et al. (2003). Four-band quantum well infrared photodetector array. *Infrared Physics & Technology*, Vol.44, No.5-6, 369-375.

Breiter, R.; Cabanski, W.A.; Mauk, K.-H.; Rode, W.; Ziegler, J.; Schneider, H. & Walther, M. (2002). Multicolor and dual-band IR camera for missile warning and automatic target recognition, In: *Targets and Backgrounds: Characterization and Representation VIII*, Watkins, W.R. et al. (Eds.),Vol. SPIE-4718, pp. 280-288, The International Society for Optical Engineering, Bellingham, WA.

Cavanillas, J.A. (1999). *The role of color and false color in object recognition with degraded and non-degraded images*. (Master's thesis) Monterey, CA: Naval Postgraduate School.

Chen, Y. & Blum, R.S. (2009). A new automated quality assessment algorithm for image fusion. *Image and Vision Computing*, Vol.27, No.10, 1421-1432.

Chen, Y., Xue, Z. & Blum, R.S. (2008). Theoretical analysis of an information-based quality measure for image fusion. *Information Fusion*, Vol.9, No.2, 161-175.

Cho, E.; McQuiston, B.K.; Lim, W.; Rafol, S.B.; Hanson, C.; Nguyen, R. & Hutchinson, A. (2003). Development of a visible-NIR/LWIR QWIP sensor, In: *Infrared Technology and Applications XXIX*, Andresen, B.F. & Fulop, G.F. (Eds.),Vol. SPIE-5074, pp. 735-744, The International Society for Optical Engineering, Bellingham,WA.

Cohen, N., Mizrahni, G., Sarusi, G. & Sa'ar, A. (2005). Integrated HBT/QWIP structure for dual color imaging. *Infrared Physics & Technology*, Vol.47, No.1-2, 43-52.

Driggers, R.G.; Krapels, K.A.; Vollmerhausen, R.H.; Warren, P.R.; Scribner, D.A.; Howard, J.G.; Tsou, B.H. & Krebs, W.K. (2001). Target detection threshold in noisy color imagery, In: *Infrared Imaging Systems: Design, Analysis, Modeling, and Testing XII*, Holst, G.C. (Eds.),Vol. SPIE-4372, pp. 162-169, The International Society for Optical Engineering, Bellingham, WA.

Essock, E.A., Sinai, M.J., McCarley, J.S., Krebs, W.K. & DeFord, J.K. (1999). Perceptual ability with real-world nighttime scenes: image-intensified, infrared, and fused-color imagery. *Human Factors*, Vol.41, No.3, 438-452.

Fay, D.A.; Waxman, A.M.; Aguilar, M.; Ireland, D.B.; Racamato, J.P.; Ross, W.D.; Streilein, W. & Braun, M.I. (2000a). Fusion of 2- /3- /4-sensor imagery for visualization, target learning, and search, In: *Enhanced and Synthetic Vision 2000*, Verly, J.G. (Eds.),Vol. SPIE-4023, pp. 106-115, SPIE -The International Society for Optical Engineering, Bellingham, WA, USA.

Fay, D.A.; Waxman, A.M.; Aguilar, M.; Ireland, D.B.; Racamato, J.P.; Ross, W.D.; Streilein, W. & Braun, M.I. (2000b). Fusion of multi-sensor imagery for night vision: color visualization, target learning and search, In: *Proceedings of the 3rd International Conference on Information Fusion*, Vol. I, pp. TuD3-3-TuD3-10, ONERA, Paris, France.

Folk, C.L. & Remington, R. (1998). Selectivity in distraction by irrelevant featural singletons: evidence for two forms of attentional capture. *Journal of Experimental Psychology: Human Perception and Performance*, Vol.24, No.3, 847-858.

Fredembach, C. & Süsstrunk, S. (2008). Colouring the near-infrared, In: *Proceedings of the IS&T/SID 16th Color Imaging Conference*, pp. 176-182.

Gegenfurtner, K.R. & Rieger, J. (2000). Sensory and cognitive contributions of color to the recognition of natural scenes. *Current Biology*, Vol.10, No.13, 805-808.

Goffaux, V., Jacques, C., Mouraux, A., Oliva, A., Schyns, P. & Rossion, B. (2005). Diagnostic colours contribute to the early stages of scene categorization: Behavioural and neurophysiological evidence. *Visual Cognition*, Vol.12, No.6, 878-892.

Goldberg, A.C., Uppal, P. & Winn, M. (2003). Detection of buried land mines using a dual-band LWIR/LWIR QWIP focal plane array. *Infrared Physics & Technology*, Vol.44, No.5-6, 427-437.

Gouras,P. (1991). Color vision. In E.R.Kandel, J.H.Schwartz, & T.M.Jessel (Eds.), *Principles of Neural Science, 3rd ed.* (pp. 467-480). Oxford, UK: Elsevier.

Gove, A.N.; Cunningham, R.K. & Waxman, A.M. (1996). Opponent-color visual processing applied to multispectral infrared imagery, In: *Proceedings of 1996 Meeting of the IRIS*

Specialty Group on Passive Sensors, Vol. II, pp. 247-262, Infrared Information Analysis Center, ERIM, Ann Arbor, US.

Green, B.F. & Anderson, L.K. (1956). Colour coding in a visual search task. *Journal of Experimental Psychology*, Vol.51, No., 19-24.

Grossberg, S. (1988). *Neural networks and natural intelligence.* MIT Press, ISBN , Cambridge, MA.

Hogervorst, M.A. & Toet, A. (2008a). Method for applying daytime colors to nighttime imagery in realtime, In: *Multisensor, Multisource Information Fusion: Architectures, Algorithms, and Applications 2008*, Dasarathy, B.V. (Eds.),Vol. SPIE-6974, pp. 697403-1-697403-9, The International Society for Optical Engineering, Bellingham, WA, USA.

Hogervorst, M.A. & Toet, A. (2008b). Presenting nighttime imagery in daytime colours, In: *Proceedings of the 11th International Conference on Information Fusion*, pp. 706-713, International Society of Information Fusion, Cologne, Germany.

Hogervorst, M.A. & Toet, A. (2010). Fast natural color mapping for night-time imagery. *Information Fusion*, Vol.11, No.2, 69-77.

Hogervorst,M.A., Toet,A., & Kooi,F.L. (2006). TNO Defense Security and Safety. Method and system for converting at least one first-spectrum image into a second-spectrum image. Patent Number Patent Number PCT/NL2007050392. Patent Application Number Application Number 0780855.5-2202 .

Howard, J.G.; Warren, P.; Klien, R.; Schuler, J.; Satyshur, M.; Scribner, D. & Kruer, M.R. (2000). Real-time color fusion of E/O sensors with PC-based COTS hardware, In: *Targets and Backgrounds VI: Characterization, Visualization, and the Detection Process*, Watkins, W.R. et al. (Eds.),Vol. SPIE-4029, pp. 41-48, The International Society for Optical Engineering, Bellingham, WA.

Huang, G., Ni, G. & Zhang, B. (2007). Visual and infrared dual-band false color image fusion method motivated by Land's experiment. *Optical Engineering*, Vol.46, No.2, 027001-1-027001-10.

Jacobson, N.P. & Gupta, M.R. (2005). Design goals and solutions for display of hyperspectral images. *IEEE Transactions on Geoscience and Remote Sensing*, Vol.43, No.11, 2684-2692.

Jacobson, N.P., Gupta, M.R. & Cole, J.B. (2007). Linear fusion of image sets for display. *IEEE Transactions on Geoscience and Remote Sensing*, Vol.45, No.10, 3277-3288.

Joseph, J.E. & Proffitt, D.R. (1996). Semantic versus perceptual influences of color in object recognition. *Journal of Experimental Psychology: Learning, Memory, and Cognition*, Vol.22, No.2, 407-429.

Kolar, R., Kubecka, L. & Jan, J. (2008). Registration and fusion of the autofluorescent and infrared retinal images. *International Journal of Biomedical Imaging*, Vol.2008, No.1-513478, 1-11.

Krebs, W.K.; Scribner, D.A.; Miller, G.M.; Ogawa, J.S. & Schuler, J. (1998). Beyond third generation: a sensor-fusion targeting FLIR pod for the F/A-18, In: *Sensor Fusion: Architectures, Algorithms, and Applications II*, Dasarathy, B.V. (Eds.),Vol. SPIE-3376, pp. 129-140, International Society for Optical Engineering, Bellingham, WA, USA.

Laliberté,F., & Gagnon,L. (2006). Studies on registration and fusion of retinal images. In R.S.Blum & Z.Liu (Eds.), *Multi-Sensor Image Fusion and its Applications.* (pp. 57-106). Boca Raton, Florida, USA: Taylor & Francis CRC Press.

Laliberté, F.; Gagnon, L. & Sheng, Y. (2002). Registration and fusion of retinal images: a comparative study, In: *International Conference on Pattern Recognition 2002*, Vol. 1, pp. 715-718, IEEE Computer Society, Washington, DC, USA.

Laliberté, F., Gagnon, L. & Sheng, Y. (2003). Registration and fusion of retinal images - an evaluation study. *IEEE Transactions on Medical Imaging*, Vol.22, No.5, 661-673.

Li, G. & Wang, K. (2007). Applying daytime colors to nighttime imagery with an efficient color transfer method, In: *Enhanced and Synthetic Vision 2007*, Verly, J.G. & Guell, J.J. (Eds.),Vol. SPIE-6559, pp. 65590L-1-65590L-12, The International Society for Optical Engineering, Bellingham, MA.

Li, J.; Pan, Q.; Yang, T. & Cheng, Y. (2004). Color based grayscale-fused image enhancement algorithm for video surveillance, In: *Proceedings of the Third International Conference on Image and Graphics (ICIG'04)*, pp. 47-50, IEEE Press, Washington, USA.

Newman, E.A. & Hartline, P.H. (1981). Integration of visual and infrared information in bimodal neurons of the rattlesnake optic tectum. *Science*, Vol.213, No., 789-791.

Newman, E.A. & Hartline, P.H. (1982). The infrared "vision" of snakes. *Scientific American*, Vol.246, No.3, 116-127.

Oliva, A. (2005). Gist of a scene, In: *Neurobiology of Attention*, Itti, L. et al. (Eds.), pp. 251-256, Academic Press.

Oliva, A. & Schyns, P.G. (2000). Diagnostic colors mediate scene recognition. *Cognitive Psychology*, Vol.41, No., 176-210.

Reinhard, E., Ashikhmin, M., Gooch, B. & Shirley, P. (2001). Color transfer between images. *IEEE Computer Graphics and Applications*, Vol.21, No.5, 34-41.

Roth, L.S.V. & Kelber, A. (2006). Nocturnal colour vision in geckos. *Proceedings of the Royal Society of London B: Biological Sciences*, Vol.271, No.Biology Letters Supplement 6, S485-S487.

Rousselet, G.A., Joubert, O.R. & Fabre-Thorpe, M. (2005). How long to get the "gist" of real-world natural scenes? *Visual Cognition*, Vol.12, No.6, 852-877.

Ruderman, D.L., Cronin, T.W. & Chiao, C.-C. (1998). Statistics of cone responses to natural images: implications for visual coding. *Journal of the Optical Society of America A*, Vol.15, No.8, 2036-2045.

Sampson, M.T. (1996). *An assessment of the impact of fused monochrome and fused color night vision displays on reaction time and accuracy in target detection* (Report AD-A321226). Monterey, CA: Naval Postgraduate School.

Schaul, L.; Fredembach, C. & Süsstrunk, S. (2009). Color image dehazing using the near-infrared, In: *Procedings of the IEEE International Conference on Image Processing ICIP2009*, pp. 1629-1632, IEEE Press, Cairo, Egypt.

Schiller, P.H. (1982). Central connections of the retinal ON and OFF pathways. *Nature*, Vol.297, No.5867, 580-583.

Schiller, P.H. (1984). The connections of the retinal on and off pathways to the lateral geniculate nucleus of the monkey. *Vision Research*, Vol.24, No.9, 923-932.

Schiller, P.H. (1992). The ON and OFF channels of the visual system. *Trends in Neuroscience*, Vol.15, No.3, 86-92.

Schiller, P.H. & Logothetis, N.K. (1990). The color-opponent and broad-band channels of the primate visual system. *Trends in Neuroscience*, Vol.13, No.10, 392-398.

Schiller, P.H., Sandell, J.H. & Maunsell, J.H. (1986). Functions of the ON and OFF channels of the visual system. *Nature*, Vol.322, No.6082, 824-825.

Schuler, J.; Howard, J.G.; Warren, P.; Scribner, D.A.; Klien, R.; Satyshur, M. & Kruer, M.R. (2000). Multiband E/O color fusion with consideration of noise and registration, In: *Targets and Backgrounds VI: Characterization, Visualization, and the Detection Process*, Watkins, W.R. et al. (Eds.),Vol. SPIE-4029, pp. 32-40, The International Society for Optical Engineering, Bellingham, WA, USA.

Scribner, D.; Schuler, J.M.; Warren, P.; Klein, R. & Howard, J.G. (2003). Sensor and image fusion, In: *Encyclopedia of optical engineering*, Driggers, R.G. (Eds.), pp. 2577-2582, Marcel Dekker Inc., New York, USA.

Scribner, D.; Warren, P. & Schuler, J. (1999). Extending color vision methods to bands beyond the visible, In: *Proceedings of the IEEE Workshop on Computer Vision Beyond the Visible Spectrum: Methods and Applications*, pp. 33-40, Institute of Electrical and Electronics Engineers.

Sévigny, L. (1996). *Multisensor image fusion for detection and recognition of targets in the battlefield of the future* (Report Progress Report Canada, NATO AC/243, Panel 3, RSG.9 37th meeting). Quebec, Canada: Defense Research Establishment Valcartier.

Shi, J.; Jin, W.; Wang, L. & Chen, H. (2005a). Objective evaluation of color fusion of visual and IR imagery by measuring image contrast, In: *Infrared Components and Their Applications*, Gong, H. et al. (Eds.),Vol. SPIE-5640, pp. 594-601, The International Society for Optical Engineering, Bellingham, MA.

Shi, J.-S., Jin, W.-Q. & Wang, L.-X. (2005b). Study on perceptual evaluation of fused image quality for color night vision. *Journal of Infrared and Millimeter Waves*, Vol.24, No.3, 236-240.

Simard, P.; Link, N.K. & Kruk, R.V. (1999). Feature detection performance with fused synthetic and sensor images, In: *Proceedings of the 43rd Annual Meeting of the Human Factors and Ergonomics Society*, pp. 1108-1112, Human Factors and Ergonomics Society.

Simard, P.; Link, N.K. & Kruk, R.V. (2000). Evaluation of algorithms for fusing infrared and synthetic imagery, In: *Enhanced and Synthetic Vision 2000*, Verly, J.G. (Eds.),Vol. SPIE-4023, pp. 127-138, The International Society for Optical Engineering, Bellingham, WA.

Sinai, M.J.; McCarley, J.S. & Krebs, W.K. (1999a). Scene recognition with infra-red, low-light, and sensor fused imagery, In: *Proceedings of the IRIS Specialty Groups on Passive Sensors*, pp. 1-9, IRIS, Monterey, CA.

Sinai, M.J.; McCarley, J.S.; Krebs, W.K. & Essock, E.A. (1999b). Psychophysical comparisons of single- and dual-band fused imagery, In: *Enhanced and Synthetic Vision 1999*, Verly, J.G. (Eds.),Vol. SPIE-3691, pp. 176-183, The International Society for Optical Engineering, Bellingham, WA.

Spence, I., Wong, P., Rusan, M. & Rastegar, N. (2006). How color enhances visual memory for natural scenes. *Psychological Science*, Vol.17, No.1, 1-6.

Sun, S., Jing, Z., Li, Z. & Liu, G. (2005). Color fusion of SAR and FLIR images using a natural color transfer technique. *Chinese Optics Letters*, Vol.3, No.4, 202-204.

Toet, A. (2003). Natural colour mapping for multiband nightvision imagery. *Information Fusion*, Vol.4, No.3, 155-166.

Toet, A. & IJspeert, J.K. (2001). Perceptual evaluation of different image fusion schemes, In: *Signal Processing, Sensor Fusion, and Target Recognition X*, Kadar, I. (Eds.),Vol. SPIE-

4380, pp. 436-441, The International Society for Optical Engineering, Bellingham, WA.

Toet, A., IJspeert, J.K., Waxman, A.M. & Aguilar, M. (1997). Fusion of visible and thermal imagery improves situational awareness. *Displays*, Vol.18, No.2, 85-95.

Toet, A. & Walraven, J. (1996). New false colour mapping for image fusion. *Optical Engineering*, Vol.35, No.3, 650-658.

Tsagaris, V. (2009). Objective evaluation of color image fusion methods. *Optical Engineering*, Vol.48, No.066201.

Tsagaris, V. & Anastasopoulos, D. (2006). Multispectral image fusion for improved RGB representation based on perceptual attributes. *International Journal of Remote Sensing*, Vol.26, No.15, 3241-3254.

Tsagaris, V. & Anastassopoulos, V. (2006). Assessing information content in color images. *Journal of Electronic Imaging*, Vol.14, No.4, 043007-1-043007-10.

Tsagiris, V. & Anastassopoulos, V. (2005). Fusion of visible and infrared imagery for night color vision. *Displays*, Vol.26, No.4-5, 191-196.

Vargo, J.T. (1999). *Evaluation of operator performance using true color and artificial color in natural scene perception* (Report AD-A363036). Monterey, CA: Naval Postgraduate School.

Walls, G.L. (2006). *The vertebrate eye and its adaptive radiation.* Cranbrook Institute of Science, ISBN , Bloomfield Hills, Michigan.

Wang, L.; Jin, W.; Gao, Z. & Liu, G. (2002). Color fusion schemes for low-light CCD and infrared images of different properties, In: *Electronic Imaging and Multimedia Technology III*, Zhou, L. et al. (Eds.),Vol. SPIE-4925, pp. 459-466, The International Society for Optical Engineering, Bellingham, WA.

Warren, P., Howard, J.G., Waterman, J., Scribner, D.A. & Schuler, J. (1999). *Real-time, PC-based color fusion displays* (Report A073093). Washington, DC: Naval Research Lab.

Waxman, A.M., et al. (1999). Solid-state color night vision: fusion of low-light visible and thermal infrared imagery. *MIT Lincoln Laboratory Journal*, Vol.11, No., 41-60.

Waxman, A.M.; Carrick, J.E.; Fay, D.A.; Racamato, J.P.; Augilar, M. & Savoye, E.D. (1996a). Electronic imaging aids for night driving: low-light CCD, thermal IR, and color fused visible/IR, In: *Proceedings of the SPIE Conference on Transportation Sensors and Controls*, Vol. SPIE-2902, The International Society for Optical Engineering, Bellingham, WA.

Waxman, A.M.; Fay, D.A.; Gove, A.N.; Seibert, M.C.; Racamato, J.P.; Carrick, J.E. & Savoye, E.D. (1995a). Color night vision: fusion of intensified visible and thermal IR imagery, In: *Synthetic Vision for Vehicle Guidance and Control*, Verly, J.G. (Eds.),Vol. SPIE-2463, pp. 58-68, The International Society for Optical Engineering, Bellingham, WA.

Waxman, A.M., Gove, A.N., Fay, D.A., Racamoto, J.P., Carrick, J.E., Seibert, M.C. & Savoye, E.D. (1997). Color night vision: opponent processing in the fusion of visible and IR imagery. *Neural Networks*, Vol.10, No.1, 1-6.

Waxman, A.M.; Gove, A.N.; Seibert, M.C.; Fay, D.A.; Carrick, J.E.; Racamato, J.P.; Savoye, E.D.; Burke, B.E.; Reich, R.K. et al. (1996b). Progress on color night vision: visible/IR fusion, perception and search, and low-light CCD imaging, In: *Enhanced and Synthetic Vision 1996*, Verly, J.G. (Eds.),Vol. SPIE-2736, pp. 96-107, The International Society for Optical Engineering, Bellingham, WA.

Waxman, A.M., Seibert, M.C., Gove, A.N., Fay, D.A., Bernardon, A.M., Lazott, C., Steele, W.R. & Cunningham, R.K. (1995b). Neural processing of targets in visible, multispectral IR and SAR imagery. *Neural Networks*, Vol.8, No.7/8, 1029-1051.

White, B.L. (1998). *Evaluation of the impact of multispectral image fusion on human performance in global scene processing*. (M.Sc.) Monterey, CA: Naval Postgraduate School.

Wichmann, F.A., Sharpe, L.T. & Gegenfurtner, K.R. (2002). The contributions of color to recognition memory for natural scenes. *Journal of Experimental Psychology: Learning, Memory, and Cognition*, Vol.28, No.3, 509-520.

Yin, S., Cao, L., Ling, Y. & Jin, G. (2010). One color contrast enhanced infrared and visible image fusion method. *Infrared Physics & Technology*, Vol.53, No.2, 146-150.

Zheng, Y. & Essock, E.A. (2008). A local-coloring method for night-vision colorization utilizing image analysis and fusion. *Information Fusion*, Vol.9, No.2, 186-199.

Zheng, Y.; Hansen, B.C.; Haun, A.M. & Essock, E.A. (2005). Coloring night-vision imagery with statistical properties of natural colors by using image segmentation and histogram matching, In: *Color imaging X: processing, hardcopy and applications*, Eschbach, R. & Marcu, G.G. (Eds.),Vol. SPIE-5667, pp. 107-117, The International Society for Optical Engineering, Bellingham, WA.

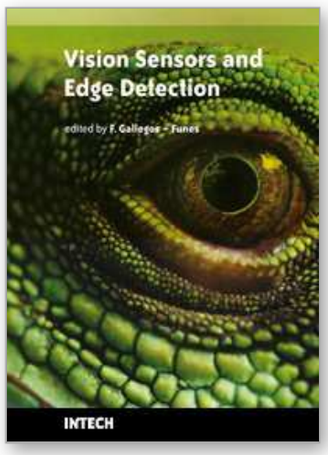

Vision Sensors and Edge Detection
Edited by Francisco Gallegos-Funes

ISBN 978-953-307-098-8
Hard cover, 196 pages
Publisher Sciyo
Published online 12, August, 2010
Published in print edition August, 2010

Vision Sensors and Edge Detection book reflects a selection of recent developments within the area of vision sensors and edge detection. There are two sections in this book. The first section presents vision sensors with applications to panoramic vision sensors, wireless vision sensors, and automated vision sensor inspection, and the second one shows image processing techniques, such as, image measurements, image transformations, filtering, and parallel computing.

How to reference
In order to correctly reference this scholarly work, feel free to copy and paste the following:

Alexander Toet and Maarten Hogervorst (2010). Real-Time Full Color Multiband Night Vision, Vision Sensors and Edge Detection, Francisco Gallegos-Funes (Ed.), ISBN: 978-953-307-098-8, InTech, Available from: http://www.intechopen.com/books/vision-sensors-and-edge-detection/real-time-full-color-multiband-night-vision

INTECH
open science | open minds

InTech Europe
University Campus STeP Ri
Slavka Krautzeka 83/A
51000 Rijeka, Croatia
Phone: +385 (51) 770 447
Fax: +385 (51) 686 166
www.intechopen.com

InTech China
Unit 405, Office Block, Hotel Equatorial Shanghai
No.65, Yan An Road (West), Shanghai, 200040, China
中国上海市延安西路65号上海国际贵都大饭店办公楼405单元
Phone: +86-21-62489820
Fax: +86-21-62489821

IntechOpen